Geophys. J. R. astr. Soc. (1982) **69**, 763–802

Magnetic properties and opaque mineralogy of drilled submarine intrusive rocks

David J. Dunlop *Université de Paris VI and CNRS Laboratoire de Géomagnétisme, 94100 St-Maur-des-Fossés, France, and Geophysics Laboratory, Department of Physics and Erindale College, University of Toronto, Toronto M5S 1A7, Canada*

Michel Prévot *Université de Paris VI and CNRS Laboratoire de Géomagnétisme, 94100 St-Maur-des Fossés, France, and United States Geological Survey, Menlo Park, California 94025, USA*

Received 1981 October 6; in original form 1981 June 4

Summary. Measurements of natural remanent magnetization (nrm), Curie temperature, ferrimagnetic and paramagnetic susceptibility, saturation induced and remanent magnetizations, coercive forces, alternating field properties and viscous magnetization are reported for 50 submarine intrusive rocks drilled during Legs 30, 37 and 45 of DSDP. The collection includes doleritic sill rocks, fresh and serpentinized cumulate gabbros and serpentinized cumulate peridotites, and serpentinized lherzolites believed to have originated in Layers 2B, 3B and 4 respectively. Magnetite, with a Curie temperature between 520 and 580°C, is the principal magnetic mineral in all samples. There is no indication of maghemitization or of metamorphism to greenschist facies or above. The magnetite in the doleritic and cumulate gabbros is a product of deuteric alteration of titanomagnetite and pyroxene; the stable nrm is a primary trm. The magnetite in the serpentinized rocks is a secondary product of serpentinization; the stable nrm is a crm. In most rock types, the magnetite is of single-domain or pseudo-single-domain size and soft components of nrm are small. The magnetite grain size in some of the doleritic gabbros is much coarser; these rocks acquire large viscous magnetizations, which however are readily removed by alternating field cleaning. The cleaned nrms of Legs 30 and 45 rocks have approximately dipole inclinations but the nrms of most of the mutually intruded Leg 37 units have been dispersed by tectonic rotations. The doleritic gabbros and the serpentinized peridotites have stable, directionally coherent nrms $\gtrsim 10^{-3}$ emu cm^{-3} in intensity. Their counterparts in Layers 2B and 3B/4 are likely contributors to oceanic magnetic anomalies. Layer 3B cumulate gabbros and tectonic serpentinites in the middle and upper crust are less likely anomaly sources.

1 Introduction

In the search for the source of linear magnetic anomalies over the ocean basins, attention has

focussed on submarine basalts to the virtual exclusion of the compositionally equivalent intrusive and plutonic rocks that make up the bulk of the oceanic crust. A decade ago this bias was understandable. The first extensive magnetic study of dredge samples of Layer 2A basalts from the North Atlantic (Irving, Robertson & Aumento 1970) showed that these rocks were so intensely magnetized that a few-hundred-metre basalt veneer seemed sufficient to account for magnetic 'stripe' anomalies (Vine & Wilson 1965).

As a result of more extensive dredging (see Prévot & Grommé 1975) and deep drilling during several legs of the Deep Sea Drilling Project (DSDP) (see Hall 1976), it is now clear that except in the axial zone of mid-ocean rifts, very intense magnetizations are *not* typical of near-surface basalts. Alteration of primary titanomagnetite to titanomaghemite with much reduced natural remanent magnetization (nrm) due to long-term exposure to seawater appears to be the norm. The mean nrm intensity of drilled DSDP basalts is about five times too weak to explain magnetic anomaly amplitudes if a 0.5 km thick source layer is assumed (Harrison 1976; Lowrie 1977).

The alternative explanation, which is the hypothesis tested in this paper, is that part of the anomaly source is the nrm of intrusive and plutonic rocks of Layers 2B, 3 and conceivably even 4. Obtaining a representative collection of these deep crustal rocks is no easy task. A number of previous studies have used dredge-hauls from the seafloor (Irving *et al.* 1970; Kent *et al.* 1978; Caytrough 1979). Such samples tend to be more weathered than their equivalents at depth in the crust. Furthermore they are unoriented. One cannot test the directional coherence of the nrm. Other studies have examined material from ophiolite suites obducted at continental margins (Beske-Diehl & Banerjee 1979; Banerjee 1980). Because of their orogenic setting, some ophiolites have a higher metamorphic grade than one would expect 5–10 km deep in the oceanic crust, even allowing for the high geothermal gradient near mid-ocean rifts. Levi *et al.* (1978) and Banerjee (1980) have proposed rock magnetic and strontium and neodymium isotopic criteria for distinguishing ophiolites whose metamorphic grade is representative of *in situ* oceanic crust from those that have been significantly degraded by obduction-related metamorphism. Directional coherence of nrm can be tested within an exposure but unless age and tectonic rotations during emplacement are known more precisely than is usually the case, comparison between nrm direction and palaeomagnetic field direction is difficult.

Our collection comprises 50 drilled oceanic intrusive rocks from DSDP Legs 30, 37 and 45. Because of the large amount of DSDP drill core available, we were able to examine 15, 26 and nine samples respectively from the three legs. The rocks were sampled at comparatively shallow depths in the crust (≤ 120 m) and except for the Leg 30 sill must have been

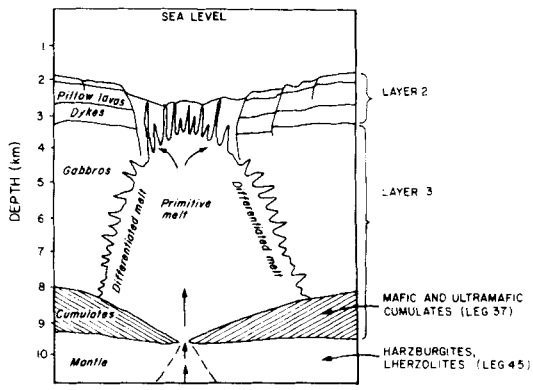

Figure 1. Structural model of a mid-oceanic ridge, after Bryan & Moore (1977).

tectonically emplaced, presumably by block-faulting in the crestal mountains bounding the axial zone. Like basalts at similar depths, they have been exposed to sea-water circulating in the crust but probably to a lesser extent than rocks exposed on the sea-bed.

Silicate mineralogy and location of each sample, geographically and in the drill core, are summarized in Table 1. Thin sections were kindly examined by Cathérine Mével, Laboratoire de Pétrographie, Université de Paris VI, who offers the following descriptions.

Leg 30, site 286 (16° 32′ S, 166° 22′ E; margin of the Indian plate, north of New Caledonia). These 15 samples are from a sill drilled within a supposed middle Eocene crust. They are gabbros with typical doleritic structure. Although the 'Initial Core Descriptions' for Leg 30 speaks of extensive chloritization and Stoeser (1975) mentions alteration in general terms, no chlorite was seen in any of the thin sections. The samples have definitely not undergone greenschist facies metamorphism. Some alteration of silicates to clay minerals is seen but many plagioclases and even olivines are fresh and intact. The mineralogy and low-temperature alteration of these samples is consistent with a shallow (Layer 2) origin from primitive undifferentiated magma.

Leg 37, site 334 (37° 02′ N, 34° 25′ W; Americas plate, 100 km west of the Mid-Atlantic Ridge). An age of about 9 Ma is deduced from magnetic stripes. These 26 samples from 10 units in the gabbro-peridotite intrusive melange of site 334 are mafic and ultramafic cumulates from a differentiated magma (Fig. 1). Units 1 and 3 comprise essentially unaltered gabbro containing two pyroxenes (one sample, 334–22–1a, has been recrystallized during deformation as described by Helmstaedt 1977). Units 2, 4, 6, 8 and 10 are serpentinized peridotites, the predominant minerals being olivine and clinopyroxene. Flower *et al.* (1977) discuss the origin and serpentinization of these rocks. Units 5, 7 and 9 are gabbros containing varying amounts of olivine serpentinized to varying degrees.

Leg 45, site 395 (22° 46′ N, 46° 05′ W; Americas plate, 75 km west of the Mid-Atlantic Ridge). Crustal age is upper Miocene. These nine samples are upper-mantle peridotites containing olivine, orthopyroxene, scarce clinopyroxene and spinels. They are thus lherzolites, approaching harzburgites. All are serpentinized, but less so than Leg 37 peridotites.

The sample collection provides, in effect, a cross-section of the oceanic crust, spanning Layer 2B, Layer 3 and the uppermost mantle. The principal unanswered question is whether serpentinization, which profoundly affects magnetic properties, occurred at the $\geqslant 5$ km depths where some of these rocks originated (e.g. Lister 1972) or whether it occurred later at shallower depths.

2 Opaque mineralogy and thermomagnetic analysis

Opaque minerals were identified by microscope observation of polished thin sections, by electron microprobe analysis of oxide phases (when grains were sufficiently large and homogeneous) and by thermomagnetic analysis of 21 selected samples. Representative results are given in Plates 1–6, Fig. 2 and Tables 2 and 3. Microprobe analyses were carried out using the Camebax probe of the CNRS–BRGM at Orléans. Thermomagnetic studies used approximately 700 mg mini-cores heated and cooled in vacuum at $15^{\circ}\mathrm{C\,min^{-1}}$ in the magnetic balance of the US Geological Survey, Menlo Park, California (Doell & Cox 1967).

2.1 LEG 30 DOLERITIC GABBRO

Opaque minerals are abundant (≈ 5 per cent according to Stoeser 1975) and have a mean size of about 200 μm. Early minerals are mainly skeletal to subeuhedral titanomagnetite and ilmenite grains, their form testifying to fairly rapid cooling after emplacement at shallow

Table 1. Key to the samples and their mineralogy.

Core and section	Interval (cm)	Unit	Rock type	Major minerals
DSDP Leg 30, Site 286				
37–4a*	10–14		Doleritic gabbro	Plag,† px, ol
37–4b	105–109		Doleritic gabbro	Plag,† px, ol
37–5a	47–51		Doleritic gabbro	Plag,† px, ol
37–5b	145–149		Doleritic gabbro	Plag,† px, ol
38–1a	101–105		Doleritic gabbro	Plag,† px, ol
38–1b	142–146		Doleritic gabbro	(No thin section)
38–2a	51–54		Doleritic gabbro	Plag, px, ol
38–3a	19–23		Doleritic gabbro	Plag, px, ol
38–3b	58–62		Doleritic gabbro	(No thin section)
38–3c	104–107		Doleritic gabbro	Plag, px, ol
38–3d	134–137		Doleritic gabbro	Plag, px, ol
38–4a	14–17		Doleritic gabbro	Plag, px, ol
38–4b	44–48		Doleritic gabbro	Plag, px, ol
38–4c	95–98		Doleritic gabbro	Plag, px, ol
38–4d	145–150		Doleritic gabbro	Plag, px, ol
DSDP Leg 37, Site 334				
21–1a	19–24	1	Cumulate gabbro	Plag, cpx, opx
21–1b	40–46	1	Cumulate gabbro	Plag, cpx, opx
21–1c (unoriented)	53–58	1	Cumulate gabbro	Plag, cpx, opx
21–1d	84–89	1	Cumulate gabbro	(No thin section)
21–1e	101–108	1	Cumulate gabbro	Plag, cpx, opx
22–1a	26–34	1	Cumulate gabbro	Plag, cpx, opx (recrystallized)
22–1b	53–61	1	Cumulate gabbro	Plag, cpx, opx
22–1c	69–73	1	Cumulate gabbro	Plag, cpx, opx
22–2a	36–39	2	Cumulate peridotite (serpentinized)	01 (serpentinized), cpx, some opx
22–2b	44–48	2	Cumulate peridotite (serpentinized)	01 (serpentinized), cpx, some opx
22–2c	52–58	2	Cumulate peridotite (serpentinized)	01 (serpentinized), cpx, some opx
23–1a	91–96	3	Cumulate gabbro	Plag, cpx, opx
23–1b	128–132	3	Cumulate gabbro	Plag, cpx, opx
23–2a (unoriented)	28–34	4	Cumulate peridotite (serpentinized)	01 (serpentinized), cpx, some opx
23–2b (unoriented)	103–109	4	Cumulate peridotite (serpentinized)	01 (serpentinized), cpx, some opx
24–2a	130–133	5	Cumulate gabbro (serpentinized)	Plag, cpx, opx, rare ol (serpentinized)
24–3a	108–115	5	Cumulate gabbro (serpentinized)	Plag, cpx, opx, rare ol (serpentinized)
24–3b	139–145	5	Cumulate gabbro (serpentinized)	(No thin section)
24–4a	78–83	6	Cumulate peridotite (serpentinized)	01 (serpentinized), cpx, some opx
24–4b	100–105	7	Cumulate gabbro (serpentinized)	Plag, cpx, opx, abun. ol (serpentinized)
25–1a (unoriented)	63–69	8	Cumulate peridotite (serpentinized)	01 (serpentinized), cpx, some opx
26–1a	119–125	8	Cumulate peridotite (serpentinized)	(No thin section)
26–2a	19–25	8	Cumulate peridotite (serpentinized)	01 (serpentinized), cpx, some opx

Table 1 – *continued*

Core and section	Interval (cm)	Unit	Rock type	Major minerals
26–2b	74–81	9	Cumulate gabbro (serpentinized)	(No thin section)
26–2c	81–88	9	Cumulate gabbro (serpentinized)	Plag, cpx, opx, ol (serpentinized)
27–1a	3–12	10	Cumulate peridotite (serpentinized)	(No thin section)
DSDP Leg 45, Site 395				
18–1a	45–54		Lherzolite (serpentinized)	01 (serpentinized), opx, rare cpx
18–1b	57–63		Lherzolite (serpentinized)	01 (serpentinized), opx, rare cpx
18–1c	78–83		Lherzolite (serpentinized)	(No thin section)
18–1d	108–113		Lherzolite (serpentinized)	01 (serpentinized), opx, rare cpx
18–1e	133–136		Lherzolite (serpentinized)	01 (serpentinized), opx, rare cpx
18–2a	71–75		Lherzolite (serpentinized)	01 (serpentinized), opx, rare cpx
18–2b	80–85		Lherzolite (serpentinized)	01 (serpentinized), opx, rare cpx
18–2c	113–118		Lherzolite (serpentinized)	01 (serpentinized), opx, rare cpx
18–2d (unoriented)	147–150		Lherzolite (serpentinized)	01 (serpentinized), opx, rare cpx

* a, b, c etc. following the core and section number indicates the first, second, third, etc. sample from that core and section.
† Plag ≡ plagioclase, px ≡ pyroxene, cpx ≡ clinopyroxene, opx ≡ orthopyroxene, ol ≡ olivine.

depth. Sometimes ilmenite and titanomagnetite form a composite intergrowth (Plate 1). Even at high magnification, the ilmenite appears homogeneous, while the titanomagnetite contains exsolved lamellae of ilmenite, presumably as a result of high-temperature oxidation during initial cooling. Pyrrhotite is present in the samples closest to the chilled margin of the sill. It occurs either as discrete grains or associated with titanomagnetite.

Microprobe analysis was unsuccessful because of the inhomogeneous crystals.

Thermomagnetic studies indicate that the principal magnetic mineral is almost titanium-free magnetite. The magnetization–temperature curves are either reversible, with a Curie point of 520–550°C (e.g. 286–38–1a, Fig. 2), or somewhat irreversible, the cooling curve displaying a lower Curie point (e.g. 286–37–4a, Fig. 2).

2.2 LEG 37 CUMULATE GABBROS

Opaque minerals are scarce and fine (less than a few μm), making their identification uncertain. Sulphides and oxides seem to be present in roughly similar amounts. Pyrrhotite, chalcopyrite, chrome spinel and magnetite were tentatively identified. They occur mainly as inclusions along cleavages in pyroxene and sporadically as interstitial grains. The grains are too fine for microprobe analysis.

Thermomagnetic curves have a predominantly hyperbolic form characteristic of rocks containing so little ferrimagnetic material that paramagnetic minerals dominate the strong field magnetization. Nevertheless a significant departure from the paramagnetic curve (dashed in Fig. 2) occurs between 400 and 570°C due to a ferrimagnetic component. The estimated Curie temperature of the ferrimagnetic phase is 550–570°C, suggesting it is nearly pure magnetite.

Table 2. Opaque mineralogy and thermomagnetic analysis of selected samples.

Sample no.	Opaque minerals	Form of J_s–T curve	T_c (°C)
Leg 30 doleritic gabbros			
286–37–4a	Abun. (≥ 5 per cent) TiMt* (coarse Il lam.), Il, sulphides	Fm,† irrev.	530
286–38–1a		Fm, rev.	540–550
286–38–3a		Fm, rev.	515
286–38–4a		Fm, irrev.	520
Leg 37 cumulate gabbros			
334–21–1a	Scarce sulphides, spinels, Mt. All as fine inclusions in cleavage planes, occ. discrete grains	Pm, ≈ rev.	555
334–22–1b		Pm, irrev.	560
334–22–1c		Pm, irrev.	570
334–23–1b		Pm, rev.	565
Leg 37 serpentinized cumulate gabbros			
334–24–3a	Scarce fine sulphides, Mt. Larger spinels. Secondary Mt, sulphides	Pm, irrev.	320, 230–250 transition
334–24–3b		Fm, rev.	570
334–24–4b		Fm, rev.	570
334–26–2c		Fm, rev.	575
Leg 37 serpentinized cumulate peridotites			
334–22–2c	Primary coarse spinels. Secondary Mt, occ. sulphides	Fm, rev.	570
334–23–2b		Fm, rev.	570
334–24–4a		Fm, rev.	570
334–26–1a		Fm, rev.	565
334–26–2a		Pm + fm, irrev.	545, 290
334–27–1a		Pm, rev.	–
Leg 45 serpentinized peridotites (lherzolites)			
395–18–1a	Web-like spinels, secondary vein Mt, few sulphides, rare manganite	Fm, rev.	570
395–18–1d		Fm	575
395–18–2b		Fm, rev.	>560

* TiMt ≡ titanomagnetite, Il ≡ ilmenite, Mt ≡ magnetite.
† Fm ≡ ferrimagnetic, pm ≡ paramagnetic.

2.3 LEG 37 SERPENTINIZED GABBROS

There are two generations of opaque minerals. Primary opaques are the same as those observed in the unaltered gabbros: sulphides, magnetite and chrome spinel, the latter sometimes large enough (> 5–10 μm) for microprobe analysis, all as inclusions in the silicates. Secondary oxides and, less commonly, sulphides result from the serpentinization of olivine. The oxides are shown by microprobe analysis (Table 3) to be pure magnetite. They occur as small anhedral grains, sometimes coalescent (Plate 2). Pyrrhotite and chalcopyrite occur as scarce fine grains. Large pyrrhotite grains surrounded by magnetite are occasionally observed (Plate 3).

Three of the four thermomagnetic curves measured show a combination of paramagnetism and ferrimagnetism, the ferrimagnetic phase having a Curie point of 570–575°C, very close to that of pure magnetite (e.g. 334–24–4b, Fig. 2). The remaining sample (334–24–3a, Fig. 2) is dominated by paramagnetic phases. It contains no magnetite but instead a ferrimagnetic phase whose thermomagnetic characteristics agree with those described by Schwarz (1973) for pyrrhotite. The Curie point of 320°C is close to that of Fe_7S_8 (310–315°C) and the hump in the heating curve around 230–250°C may correspond to the γ transition of

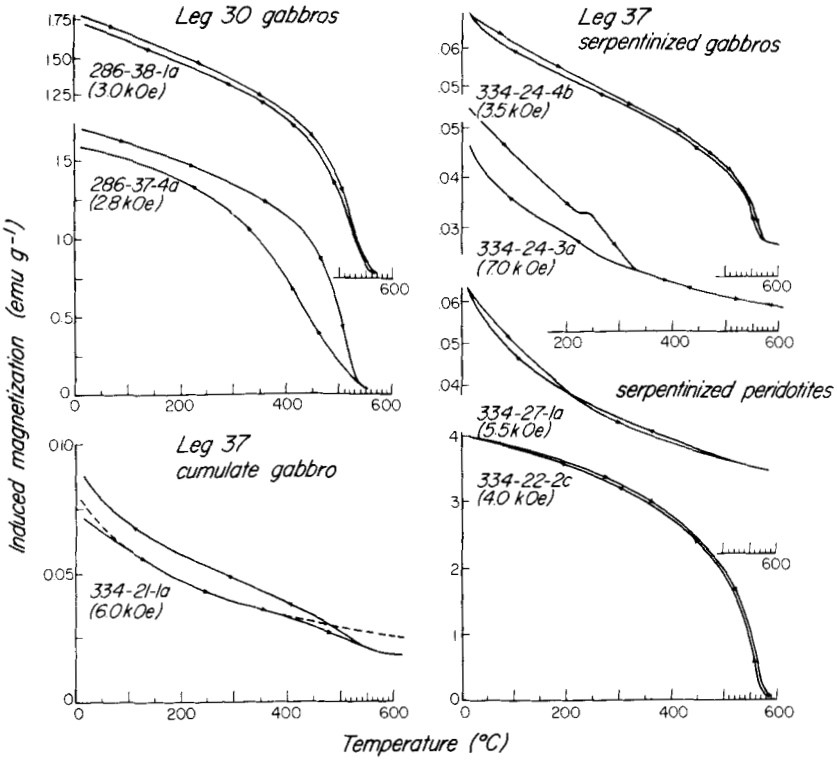

Figure 2. Representative vacuum thermomagnetic curves. Applied field: 2.5–8 kOe.

Fe_9S_{10}. Ferrimagnetic pyrrhotite is no longer detectable in the cooling curve, indicating that heating to 630°C in vacuum resulted in the breakdown of this mineral into non-magnetic phases, probably pyrite and non-magnetic pyrrhotite.

Since magnetite is by far the most abundant magnetic product of serpentinization, the predominance of pyrrhotite in 334–24–3a must be attributed to the primary mineralogy of this rock. This conclusion is confirmed by the polished thin section observations, which show that secondary oxides are absent in this sample and primary pyrrhotite within silicates is abundant. The opaque mineralogy of serpentinized olivine gabbros is thus highly variable, from virtually unaltered cumulate gabbro on the one hand to an assemblage in which secondary magnetite is the principal magnetic mineral on the other.

2.4 LEGS 37 AND 45 SERPENTINIZED PERIDOTITES

As in the serpentinized gabbros, there are two generations of opaque minerals. Primary opaques are large, often euhedral spinels up to 500 μm in size (Plate 4). Compositionally, they are magnesian chrome-picotites (Babkine *et al.* 1965). They are more abundant and more chrome-rich in Leg 37 than in Leg 45 peridotites. Coarse web-shaped chromites occur in some Leg 45 peridotites (e.g. sample 395–18–1a, Table 3 and Plate 5).

Secondary opaques are mainly magnetite (Table 3). In Leg 37 serpentinized peridotites, magnetite forms principally as fine dispersed grains and sometimes also as veinlets filling cracks in or at the boundary of primary spinels (Plate 4). In the Leg 45 samples, magnetite occurs mainly as veinlets, sometimes with an elongate core of ferrous or magnesian chrome-picotite (Table 3, Plate 6). Discrete small sulphide grains are present in both Legs 37 and 45

Table 3. Typical electron microprobe analyses of oxides in some serpentinized intrusives.

Element	Sample, mineral probed and number of analyses					
probed	334–24–3a* spinel (2 anal.)	334–26–2c sec. Mt (5 anal.)	334–22–2b sec. Mt (19 anal.)	spinel (12 anal.)	395–18–1a sec. Mt (2 anal.)	spinel (4 anal.)
SiO_2	0.32	0.81	1.26	0.07	1.10	0.04
FeO	21.42	30.11	29.55	17.47	28.37	13.87
Fe_2O_3	3.21	68.03	67.18	6.39	67.86	3.15
TiO_2	0.09	0.00	0.00	0.41	0.00	0.02
Al_2O_3	37.71	0.00	0.03	22.42	0.00	36.24
Cr_2O_3	24.72	0.00	0.12	40.77	0.09	31.03
MgO	10.23	0.27	0.47	11.62	1.18	15.43
MnO	0.20	0.00	0.03	0.49	0.01	0.30
ZnO, NiO	0.13	0.04	0.09	0.20	0.10	0.27
Total	98.03†	99.26	98.73†	99.84	98.71†	100.35

* Spinel core in magnetite filling cracks.
† Totals <99 are due to grain sizes less than electron beam size. They do not indicate vacancies in the crystal structure.

peridotites. In the Leg 37 samples, where they are more frequent, they have been identified as pentlandite (MacLean 1977). Another secondary opaque is cryptomelane, which forms large (a few hundred μm) veins in the Leg 45 serpentinites.

Thermomagnetic curves are generally reversible with a Curie point near 570°C (e.g. 334–22–2c, Fig. 2). One sample (334–27–1a) of the nine examined had a paramagnetic curve (Fig. 2), however, again pointing up the magnetic heterogeneity of serpentinized rocks.

2.5 DISCUSSION AND SUMMARY

The principal carrier of nrm in almost every submarine intrusive rock we examined is magnetite, with a Curie point between 515 and 575°C. The same observation was made by Kent *et al.* (1978) for dredged submarine gabbros, and is in marked contrast to the situation in submarine basalts, where the primary magnetic mineral is a titanium-rich titanomagnetite with an average Curie point of 160°C (Prévot, Lecaille & Hekinian 1979) to 210°C (Prévot, Lecaille & Mankinen 1981), depending on the method of determination used. An important consequence is that, unlike the Curie-point isotherm for submarine basalts, which is at the most a few kilometres deep, the Curie-point isotherm for submarine intrusives lies deep in the crust or in the upper mantle. Furthermore, the magnetites in submarine intrusive rocks do not seem to have suffered from maghemitization, which is ubiquitous in submarine basalts.

The magnetite has several different sources. In the Leg 30 doleritic gabbros, the magnetite is primary, a product of deuteric oxidation of high-titanium titanomagnetite at temperatures close to or above the Curie point of magnetite. The nrm is a primary thermoremanent magnetization (trm) or thermochemical remanence (tcrm, Grommé, Wright & Peck 1969). In the unaltered Leg 37 cumulate gabbros, the magnetite is probably a primary deuteric oxidation product of pyroxene and plagioclase. Since these reactions go to completion well above 600°C, the nrm should be a primary trm acquired during cooling. Occasionally pyrrhotite rather than magnetite is the dominant magnetic carrier, but the same conclusions about the primary nrm hold true.

Serpentinization results in the crystallization of pure magnetite, principally at temperatures between 250 and 500°C (Cann 1979). The homogeneous spinel core within some

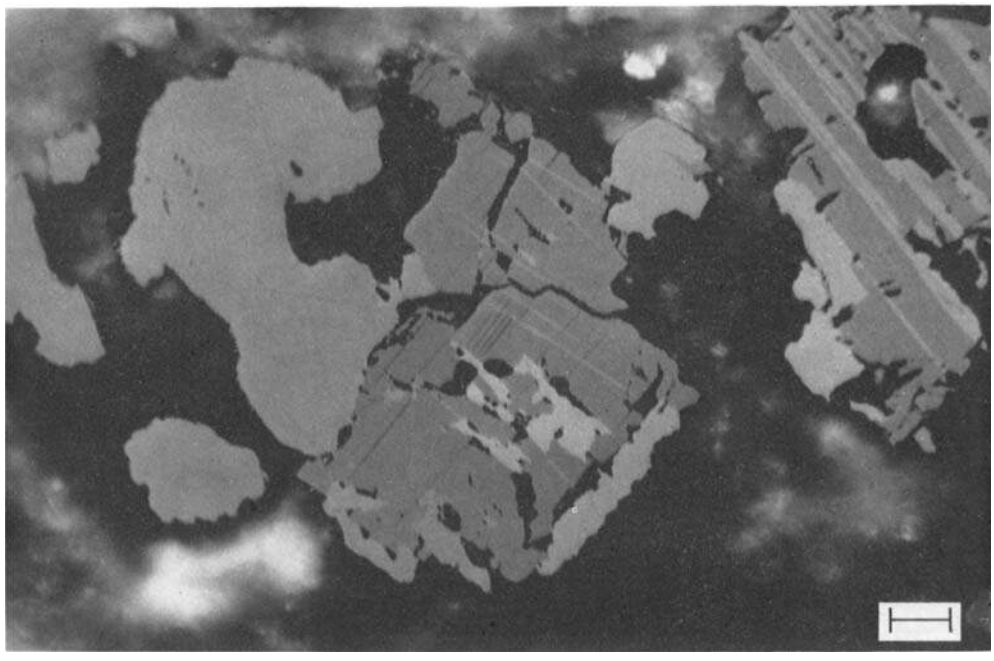

Plate 1. Doleritic gabbro 286–38–3a; parallel Nicols, oil immersion; white bar 50 μm long. Primary ilmenite (homogenous medium grey to light grey irregular areas) associated with magnetite (medium grey) subdivided by exsolution lamellae of second generation ilmenite (light to dark greys) set along (111) planes of the magnetite host.

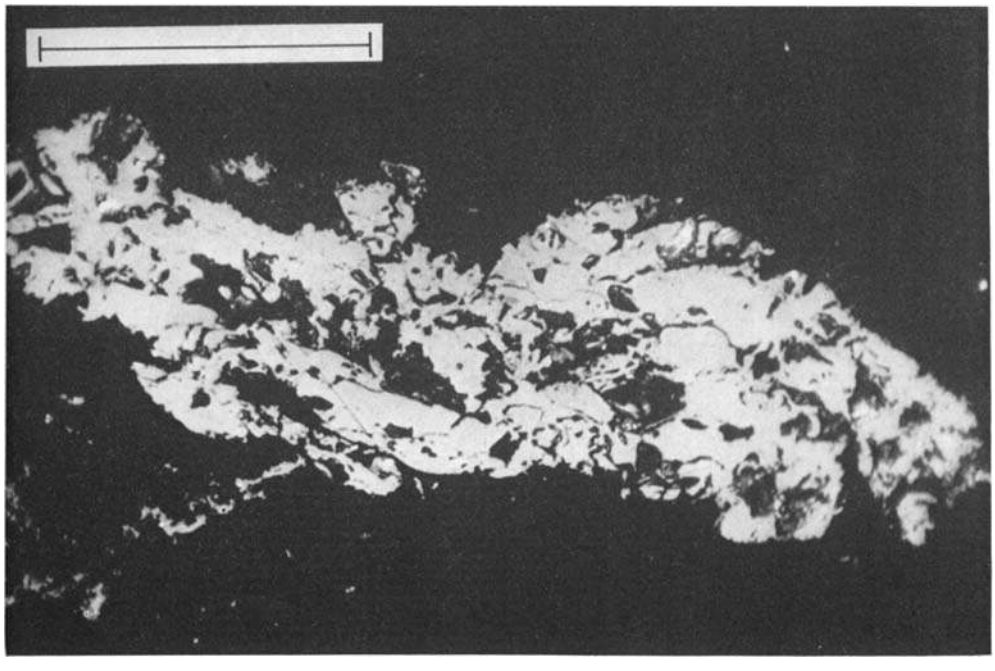

Plate 2. Serpentinized gabbro 334–26–2c; same conditions as Plate 1. Coalescent secondary magnetite grains (microprobe analysis in Table 3, column 3) after serpentinization with some fine sulphide grains (the whitest spots) partially included within the magnetite or separate (near the centre of the right margin).

[*facing page* 770]

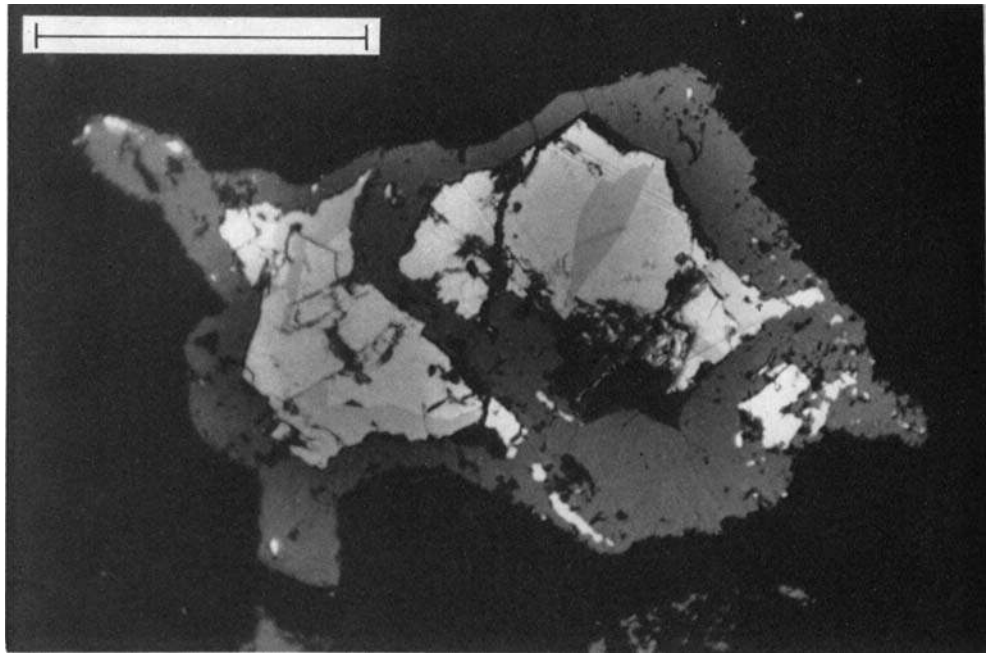

Plate 3. Same sample and conditions as Plate 2. Secondary magnetic minerals: composite intergrowth of pyrrhotite (various light greys owing to pleochroism) and magnetite (dark grey).

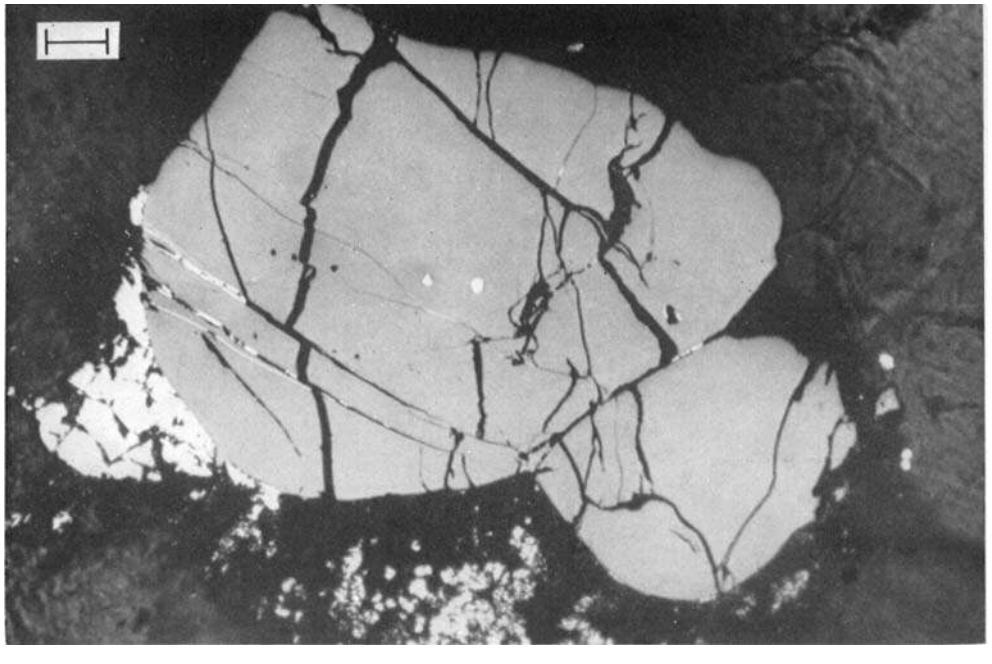

Plate 4. Serpentized peridotite 334–22–2b; same conditions as Plate 1. Earlier chrome spinel (medium grey; microprobe analyses in Table 3, column 5) and secondary magnetite (white) crystallized at the contact with or within a crack in the spinel. Finer interstitial magnetite grains near the centre of the lower margin.

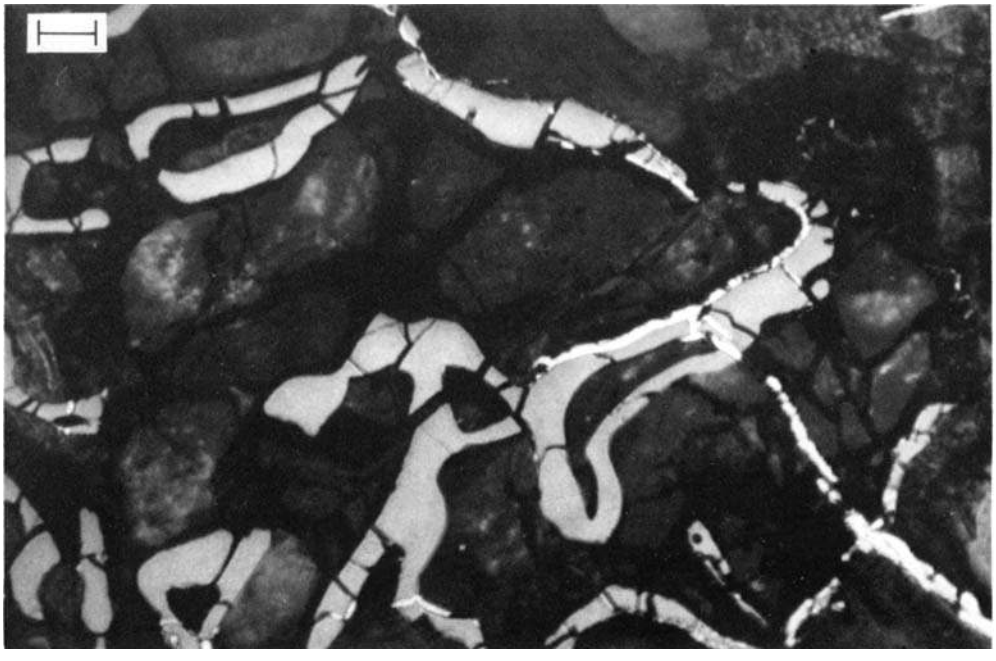

Plate 5. Serpentized peridotite 395–18–1a; same conditions as Plate 1. Web-shaped chrome spinels (medium grey, microprobe analysis in Table 3, column 7) with some secondary magnetite veinlets (white).

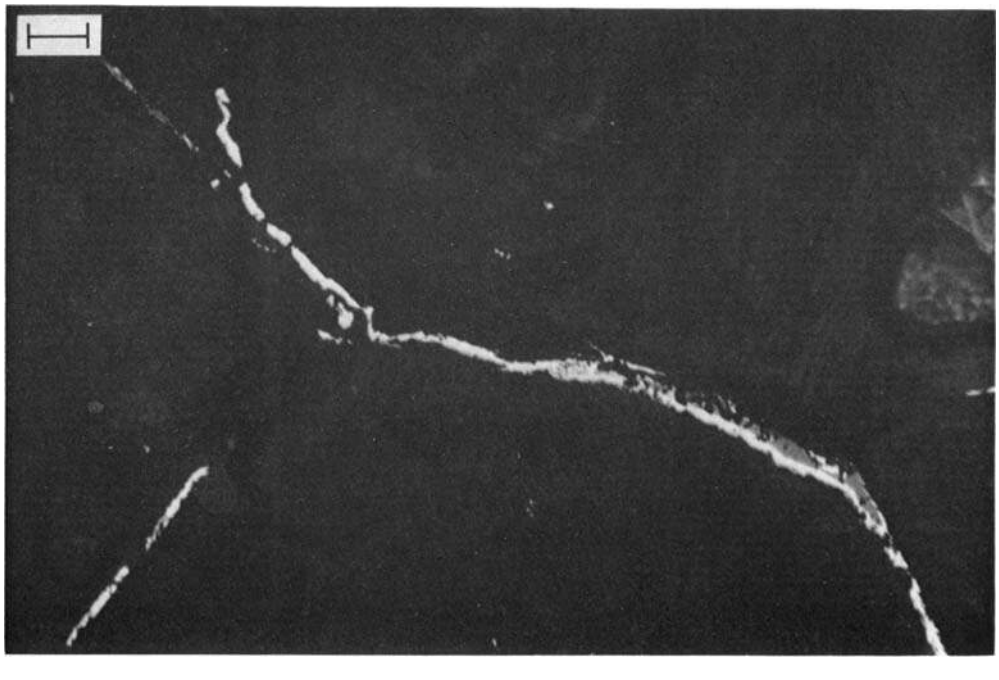

Plate 6. Same sample and conditions as Plate 5. Secondary magnetite veins (white; microprobe analysis in Table 3, column 6) with at places a core of chrome spinel (light grey).

veinlets of secondary magnetite in Leg 45 peridotites may indicate that serpentinization began at the high temperature end of this range, since complete solid solution of spinels is not obtained experimentally below 510°C (Deer, Howie & Zussman 1964). In the course of serpentinization, gabbros and peridotites acquire a crystallization remanence (crm), presumably directed along the ambient geomagnetic field at the time serpentinization occurs. For serpentinized peridotites, this crm is the only nrm, the primary chrome spinels being paramagnetic. Serpentinized gabbros, on the other hand, may carry primary trm in addition to secondary crm. Although primary magnetite and pyrrhotite are usually much less abundant than secondary magnetite in these rocks, the secondary oxides are much coarser and their remanence should be magnetically soft (easily removed by alternating field demagnetization). These predictions will be tested in Sections 3 and 4.

3 Hysteresis and domain structure

3.1 SATURATION MAGNETIZATION AND FERRIMAGNETIC MINERAL CONTENT

Induced magnetization J in strong fields was measured in two ways. The magnetization curves of 10–25 g subsamples of all 50 samples (20–70 g) were measured at St Maur in fields H up to 5 kOe, using a ballistic magnetometer with pickup coils in the gap of an electromagnet and a galvanometer amplifier. The curves of small cores (0.6–0.7 g) from 21 selected samples were determined using the Curie balance of the US Geological Survey, Menlo Park, in fields up to 9 kOe (see Fig. 3 for typical results).

The data for the 33 samples whose magnetization curves are purely ferrimagnetic were fitted to the well-known law for the approach to ferrimagnetic saturation magnetization J_s,

$$J/J_s = 1 - A/H, \qquad (1)$$

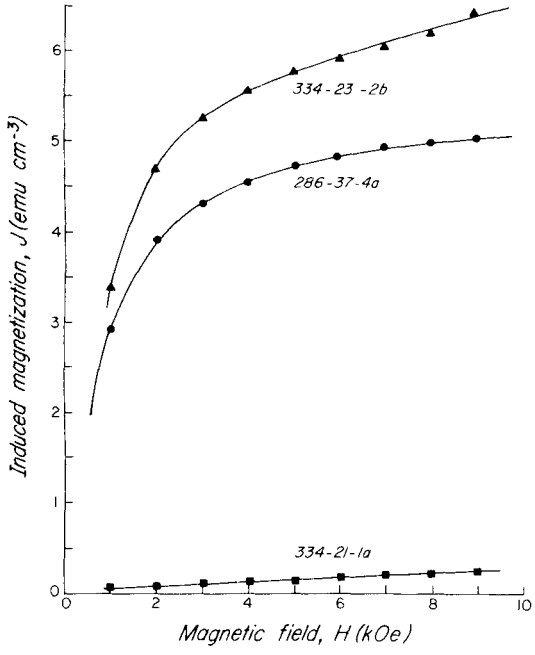

Figure 3. Typical initial magnetization curves measured at room temperature for strongly magnetic and weakly magnetic samples.

over the field range 1.5–5 kOe (St Maur data) or 3–9 kOe (Menlo Park data). Excellent fits were obtained in practically all cases and A proved to have very nearly the same value for all samples. Taking advantage of this fact, J_s as tabulated in Table 4 was obtained by multiplying measured values of J in 5 kOe by a 'universal' factor 1.08. (Individual factors ranged between extremes of 1.05 and 1.11.)

The remaining 17 samples contain such a small fraction of ferrimagnetic minerals that the magnetization of paramagnetic opaques (ilmenite, spinels) and silicates significantly affects the J–H curve. Our criterion for a significant paramagnetic contribution was that ≥ 25 per cent of J at 5 kOe be due to paramagnetic minerals, but in fact the samples were rather sharply divided into strongly magnetic (ferrimagnetic minerals > 0.25 per cent by volume, and usually ≥ 1 per cent) and weakly magnetic (ferrimagnetic content < 0.1 per cent and usually $\ll 0.1$ per cent) groups (*cf.* Fig. 3). There were no borderline cases.

The St Maur magnetization data for the weakly magnetic group of samples were fitted to the law

$$J/J_s = A/H + (k_{pm}/J_s)H, \qquad (2)$$

Table 4. Ferrimagnetic saturation magnetization J_{sat} and paramagnetic and ferrimagnetic susceptibilities k_{pm} and k_{fm}.

Sample no.	J_{sat} (emu cm^{-3})	Vol. per cent fm. minerals	$k_{pm} \times 10^6$ (emu cm^{-3} Oe^{-1})	$k_{fm} \times 10^6$ (emu cm^{-3} Oe^{-1})
Leg 30 doleritic gabbros				
286–37–4a	4.9	1.00		1800
286–38–1a	6.4	1.35		2650
286–38–1b	0.13	0.03	19.6	100
286–38–3a	6.1	1.30		4250
286–38–4a	4.6	0.95		2600
Leg 37 cumulate gabbros				
334–21–1a	0.035	<0.01	30.1 (23.8)*	41.5
334–21–1e	0.018	<0.01	(26.3)	(88.7)*
334–22–1b	0.022	<0.01	32.0 (33.6)	41.4
334–22–1c	0.031	<0.01	32.2 (32.4)	36.4
334–23–1b	0.021	<0.01	33.7 (31.6)	21.9
Leg 37 serpentinized cumulate gabbros				
334–24–3a	0.029	<0.01	21.8 (20.0)	18.9
334–24–3b	3.5	0.75		1300
334–24–4b	1.2	0.25		560
334–26–2b	0.135	0.03	(20.1)	(170)
334–26–2c	1.2	0.25		450
Leg 37 serpentinized cumulate peridotites				
334–22–2c	13.5	2.80		4500
334–23–2b	8.45	1.75		2850
334–24–4a	5.0	1.05		2100
334–26–1a	6.45	1.35		2700
334–26–2a	(0.09)	<0.01	22.5 (20.0)	?
334–27–1a	0.028	<0.01	25.8 (26.4)	22.1
Leg 45 serpentinized peridotites (lherzolites)				
395–18–1a	4.25	0.90		2800
395–18–1d	1.6	0.35		1300
395–18–2b	3.1	1.35		2900
395–18–2d	0.51	0.10	(31.2)	(200)

* Bracketed values of k_{pm} were determined from the approach to saturation magnetization below 5 kOe (see text). The comparison k_{fm} values calculated using these values are also uncertain.

where k_{pm} is the (volume) paramagnetic susceptibility. Two curve fit procedures were used. The first was a graphical method of successive approximations which assumed the 'universal' value for A found for the purely ferrimagnetic samples. The second was an analytic least-squares fitting routine that yielded J_s, k_{pm} and A. The two procedures gave indistinguishable results for both J_s and k_{pm}.

The weakly magnetic samples tend to be magnetically inhomogeneous. Subsamples of the same sample have J_s values differing typically by ≥ 20 per cent and occasionally by a factor 5. A factor 2 difference is common. Any systematic differences due to the different fields used at Menlo Park and at St Maur are insignificant compared to differences arising from spatial fluctuations in magnetic mineral concentration. Under these circumstances, the St Maur subsamples, being larger, are likely to provide more representative values of J_s and magnetic mineral content, and it is these values that are given in Table 4.

Where available, both St Maur and Menlo Park k_{pm} determinations (the latter obtained directly from the 5–9 kOe slope of the J–H curve) are quoted in Table 4. Although the St Maur values are bracketed to indicate the relative uncertainty of the curve-fit procedures, the two sets of values tend to agree quite closely.

Comparison of Fig. 2 and Table 4 demonstrates the expected correlation between paramagnetic thermomagnetic behaviour and slight ferrimagnetic contribution to the J–H curve and between ferrimagnetic J–T behaviour and strongly magnetic J–H characteristics. With two exceptions, the Legs 30 and 45 samples are strongly magnetic, containing $g \approx 1$ per cent by volume magnetite, while the Leg 37 unaltered cumulate gabbros are uniformly weakly magnetic, with ferrimagnetic contents < 0.01 per cent.

In line with their heterogeneous opaque mineralogy (Sections 2.3, 2.4), Leg 37 serpentinized gabbros and peridotites are sometimes strongly, sometimes weakly magnetic, depending on the degree of serpentinization. Samples like 334–24–3a, 26–2a and 27–1a are magnetically as weak as the unaltered gabbros and presumably lack any secondary magnetite. Samples in which serpentinization has been accompanied by secondary magnetite formation are strongly magnetic. Indeed, the Leg 37 serpentinized peridotites (units 2, 4, 6 and 8) include the most magnetic samples in our study, presumably because they contain much more olivine than the gabbros. Of the 10 samples in this group, seven have ferrimagnetic contents of 1.0–2.4 per cent.

3.2 PARAMAGNETIC AND FERRIMAGNETIC SUSCEPTIBILITIES

For the 33 strongly magnetic samples, initial susceptibility in an alternating field of ≈ 1 Oe was measured with the sample at rest in the pickup coils of a spinner magnetometer (Thellier 1967). For the 17 weakly magnetic samples, the sensitivity by this method was inadequate and initial susceptibility in a direct field of 10 Oe was measured using a ballistic magnetometer and galvanometer amplifier (see Section 3.3) and a solenoid. In the latter case, the ferrimagnetic initial susceptibility k_{fm} was obtained by subtracting k_{pm} (Section 3.1) from the total susceptibility. In strongly magnetic samples, where the ferrimagnetism swamps any paramagnetic contribution, k_{fm} is the total susceptibility as measured and k_{pm} cannot be determined.

Paramagnetic susceptibility k_{pm} ranges from $18–34 \times 10^{-6}$ emu cm^{-3} Oe^{-1} (Table 4). In the Leg 37 collection (15 of the 17 k_{pm} determinations), unaltered gabbros tend to have the higher values of k_{pm} and the serpentinized gabbros and peridotites tend to have the lower values.

Ferrimagnetic susceptibility k_{fm} ranges over almost three orders of magnitude, from 11

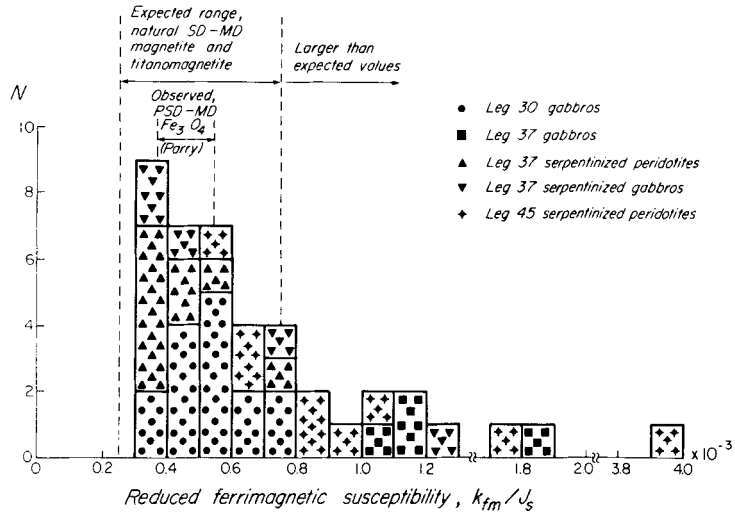

Figure 4. Histogram of reduced ferrimagnetic susceptibility. Values falling much above the expected range for SD to MD magnetite indicate superparamagnetic grains (Prévot 1981).

to 4500×10^{-6} emu cm^{-3} Oe^{-1} (Table 4). Most of this variability simply reflects varying ferrimagnetic mineral content, as evidenced by the fact that most values of k_{fm}/J_s (Fig. 4) fall in the narrow range 0.3–0.8×10^{-3} expected for single-domain (SD) or multidomain (MD) magnetite.

Two groups of rocks have consistently high values of k_{fm}/J_s, i.e. ferrimagnetic susceptibilities higher than expected for their ferrimagnetic mineral content. These are Leg 37 unaltered gabbros (all samples) and Leg 45 lightly serpentinized peridotites (six of nine samples). The probable explanation is the occurrence of superparamagnetic grains (Prévot 1981), here magnetite $< 0.03\,\mu$m in size, in both groups of rocks. A superparamagnetic fraction among the fine magnetite inclusions in Leg 37 gabbros is natural enough, but a similar fraction among the secondary magnetites in some (but not all) Leg 45 serpentinized peridotites is somewhat unexpected. It should be remembered that even trace amounts of superparamagnetic material affect k_{fm} significantly, since the superparamagnetic susceptibility is one or two orders of magnitude greater than the ordinary ferrimagnetic susceptibility (e.g. Dunlop 1974). The superparamagnetic fractions indicated by the data of Fig. 4 are only a few per cent by volume of the total ferrimagnetic content.

3.3 SATURATION REMANENCE

Saturation remanence, J_{rs}, was measured for independent subsamples either at St Maur using the instruments described in Section 3.1 after applying a field of 5 kOe or at Menlo Park using a spinner magnetometer after application of a 9 kOe field. In a few cases, the St Maur values were checked using a spinner magnetometer. Reduced saturation remanence J_{rs}/J_s is a frequently used index of domain structure. Although within-sample variation of J_s is large (Section 3.2), Menlo Park and St Maur determinations of J_{rs}/J_s for the same sample agree well. The Menlo Park values are systematically larger, indicating a closer approach to saturation. They are therefore quoted, where available, in Table 5, except in the case of sample 334–24–4b, which is exceptionally inhomogeneous.

With a few exceptions, $J_{rs}/J_s > 0.05$, the maximum value observed by Parry (1965) and Rahman, Duncan & Parry (1973) for $\geqslant 15\,\mu$m MD magnetite but $J_{rs}/J_s < 0.5$, the value for

Table 5. Representative domain structure indices of ferrimagnetic minerals from hysteresis and nrm measurements (symbols defined in the text).

Sample no.	Q_n	$\tilde{H}_{1/2}$ (Oe peak)	H_c (Oe)	H_R (Oe)	H_R/H_c	J_{rs}/J_s	Lowrie-Fuller test result
Leg 30 doleritic gabbros							
286–37–4a	7.9	153	141	248	1.76	0.16	
286–37–5a	1.2	(181)★	102	243	2.38	0.13	
286–38–1a	4.1	71	78	179	2.31	0.08	
286–38–3a	1.15	(31)	30	115	3.77	0.03	Multidomain
286–38–4a	1.15	(38)	33	96	2.91	0.04	
286–38–4c	0.65	(23)	34	97	2.85	0.045	
Leg 37 cumulate gabbros							
334–21–1a	7.7	465	(195)†	375	(1.92)‡	0.29	
334–22–1b	10.6	645	(150)	292	(1.95)	0.33	
334–22–1c	29.1	765	(190)	520	(2.74)	0.39	Single-domain
334–23–1b	12.8	580	(210)	500	(2.38)	0.32	
Leg 37 serpentinized cumulate gabbros							
334–24–3a	(0.75?)§		(620)	1055	1.70	0.56	
334–24–3b	1.2	(117)	102	166	1.63	0.18	Pseudo-single-domain
334–24–4b	4.0	(106)	147	214	1.46	0.20	
334–26–2c	3.3	(105)	128	194	1.52	0.22	
Leg 37 serpentinized cumulate peridotites							
334–22–2a	3.1	122	139	212	1.52	0.20	
334–22–2c	2.8	81	89	171	1.92	0.16	Pseudo-single-domain
334–23–2b	1.35	(110)	100	206	2.06	0.18	
334–24–4a	1.2	(85)	98	146	1.49	0.17	
334–26–1a	1.8	(109)	115	192	1.67	0.19	
334–26–2a	(1.3)		(175)	380	(2.20)	0.29	
334–27–1a	(0.45?)§		(120)	252	(2.07)	0.13	
Leg 45 serpentinized peridotites (lherzolites)							
395–18–1a	(5.9)¶	(38)	43	89	2.07	0.13	Pseudo-single-domain
395–18–1d	(4.9)¶	(32)	43	85	1.96	0.08	
395–18–2b	(7.8)¶	(34)	50	94	1.89	0.10	

★ Bracketed values of $\tilde{H}_{1/2}$ indicate a changing magnetization direction during AF demagnetization.
† Bracketed values of H_c indicate values corrected for the effect of paramagnetism by a method described in the text.
‡ Bracketed values of H_R/H_c are uncertain by virtue of the uncertainty in H_c.
§ These bracketed values of Q_n are uncertain because the samples are very inhomogeneous, and J_{nrm} and k_{fm} were determined on different subsamples.
¶ These bracketed Q_n values reflect large spurious remanences produced in the drilling operation, and are unrepresentative of the pre-drilling nrm.

SD grains with uniaxial shape anisotropy. (SD pyrrhotite can have $J_{rs}/J_s > 0.5$ due to crystalline anisotropy, as witness 334–24–3a.) Most samples therefore contain pseudo-single-domain (PSD) magnetite with grain size $0.03\,\mu m < d < 15\,\mu m$.

The magnetite inclusions in Leg 37 gabbros ($J_{rs}/J_s \gtrsim 0.3$) must be predominantly $< 0.1\,\mu m$ in size (Dunlop 1973) and probably include much true SD material. Leg 37 serpentinized rocks ($0.15 \lesssim J_{rs}/J_s < 0.3$) contain, on the whole, rather fine PSD grains, ranging from near SD size to perhaps $0.5\,\mu m$ (Dunlop 1973). Leg 45 rocks ($0.1 \lesssim J_{rs} < 0.15$) contain much coarser, probably $> 1\,\mu m$, magnetite.

Leg 30 doleritic gabbros contain the coarsest grains of all. Except for the upper few samples, which lie in the chilled margin of the sill and have J_{rs}/J_s values like the Leg 45

rocks, the Leg 30 samples have $0.03 \leqslant J_{rs}/J_s < 0.1$ and grain sizes are probably $\gtrsim 10\,\mu m$. Such large effective grain sizes are unusual in deuterically oxidized titanomagnetites. Grains are normally subdivided by ilmenite lamellae into small PSD or even SD magnetite regions (Larson *et al.* 1969).

3.4 COERCIVE FORCES

Coercive force, H_c, and remanent coercive force, H_R (the reverse field required to reduce the remanence to zero following forward saturation) were determined using a vibrating-sample magnetometer (a repeated-stroke ballistic system with galvanometer amplifier designed by A. Lecaille at St Maur), and a 1.5 kOe solenoid. This system was used in preference to the 5 kOe ballistic magnetometer/electromagnet system, described in Section 3.1, which had a substantial (≈ 100 Oe) field due to remanence of the pole pieces under nominally zero-field (i.e. zero current) conditions. The drawback of the solenoid system is its non-saturating field. Measured H_C and H_R are therefore slightly lower than saturation values and H_R/H_C may be slightly overestimated.

For the 17 weakly magnetic samples, whose paramagnetic susceptibilities were substantial fractions of total susceptibility, H_c determined directly from the hysteresis loop is unrepresentative of the ferrimagnetic minerals. (H_R, being based solely on remanence measurements, is unaffected by paramagnetic induced magnetization.) The following correction procedures were adopted. An exact graphical method is to superimpose a synthetic (linear) J–H plot for the paramagnetic minerals alone (using k_{pm} from Table 4) on the measured hysteresis loop. The intersection of the two curves yields the coercive force for the ferrimagnetic minerals alone, since this field makes $J_{total} = J_{pm}$ or $J_{fm} = 0$. Coercive forces tabulated in Table 5 were obtained in this way.

We also tested an approximate analytical method for obtaining this intersection without measuring the complete hysteresis curve. This is to assume linearity of the descending branch of the loop as H changes from 0 to $-(H_c)_{tot}$, the measured coercive force of the total magnetization J, and for a sufficient range of negative fields beyond $-(H_c)_{tot}$ to obtain the intersection point $(H_c)_{fm}$. Between 0 and $-(H_c)_{tot}$, J is reduced from J_{rs} to 0. The required linearized hysteresis loop segment is thus

$$J = J_{fm} + J_{pm} \simeq J_{rs} + [J_{rs}/(H_c)_{tot}]\,H. \tag{3}$$

The paramagnetic magnetization curve is

$$J_{pm} = k_{pm}H. \tag{4}$$

Since $H = -(H_c)_{fm}$ when $J_{fm} = 0$, i.e. when $J = J_{pm}$, (3) and (4) can be combined to give

$$(H_c)_{fm} \simeq [(H_c)_{tot}^{-1} - k_{pm}/J_{rs}]^{-1}. \tag{5}$$

Since the negative-field section of the descending hysteresis loop normally has a net upwards convexity over the range 0 to $-(H_c)_{fm}$, equation (5) tends to overestimate $(H_c)_{fm}$. Although inexact, this method of 'correcting' H_c data is quick and convenient if the hysteresis loop has not been measured (or is not given, if published data are being corrected), since only the normally measured parameters k_{pm}, J_{rs} and $(H_c)_{tot}$ are required.

Coercive forces predicted by equation (5) ranged from 5–20 per cent higher than the exact values, except in the case of 334–24–3a, where the pronounced downward convexity of the descending branch of the hysteresis curve (due to pyrrhotite) caused the analytical method to fail.

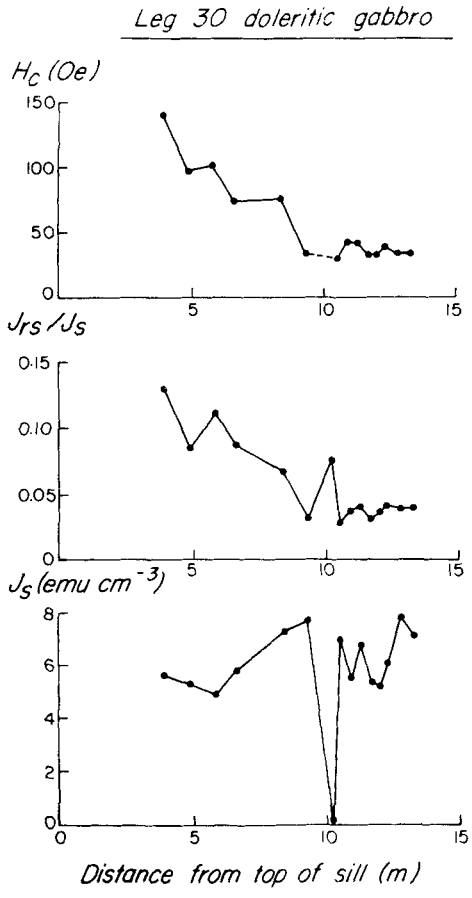

Figure 5. Variation of hysteresis properties with distance from the chilled margin of a doleritic sill. High values of H_c and J_{rs}/J_s reflect the finer grain size of the chilled zone. Magnetite content, indicated by J_s, is approximately constant throughout.

The coercive force H_c decreases in a regular fashion with distance of Leg 30 samples from the chilled top of the sill (Fig. 5). Samples in the chilled zone have coercive forces in the 75–140 Oe range, characteristic of large PSD magnetite grains from one to a few μm in size (Parry 1965). In the interior of the sill, coercive forces are uniformly about 30 Oe, indicating MD magnetite $>15\,\mu$m in size. J_{rs}/J_s values have the same trend (Section 3.3), as do other indicators of domain structure, such as H_R, H_R/H_c, $\tilde{H}_{1/2}$ (median destructive field of nrm, Section 4.4) and Q_n (Koenigsberger ratio, Section 4.5) (Table 5). J_s, on the other hand, does not vary in any systematic fashion through the sill (Fig. 5). Ferrimagnetic mineral content is comparable in the chilled margin and the interior of the sill; only grain size varies systematically.

Representative values of H_c, H_R and the ratio H_R/H_c, which is diagnostic of domain structure (Wohlfarth 1958; Gaunt 1960), are given in Table 5. Leg 45 samples, whose magnetites are in the upper PSD size range (Section 3.3), have for the most part H_c and H_R values of 40–50 Oe and 85–95 Oe respectively, fairly similar to values for the truly MD magnetites in the interior of the Leg 30 sill. However the two sets of samples have quite distinct H_R/H_c values: $H_R/H_c \gtrsim 3$ for the Leg 30 samples (MD grains) and $H_R/H_c \approx 2$ for the Leg 45 rocks (large PSD grains).

The strongly magnetic Leg 37 serpentinized gabbros and peridotites tend to have H_c = 100–150 Oe, H_R = 170–250 Oe, H_R/H_c = 1.5–2.0. Such values are characteristic of rather small (< 0.5 μm) PSD grains of magnetite (Dunlop 1973).

The weakly magnetic Leg 37 serpentinites and the unaltered gabbros (all of which are weakly magnetic) are magnetically harder. H_c ranges from 120 to 350 Oe; H_R is 250–520 Oe. For PSD grains close to SD size, perhaps incorporating some SD material (Section 3.3) the H_R/H_c values are surprisingly high: 1.4–2.7, with the majority of values $\gtrsim 2$. Such H_R/H_c values usually characterize large PSD grains of magnetite (Parry 1965). Sample 334–24–3a is unique in our collection in that its magnetic properties are dominated by SD pyrrhotite. H_c and H_R are large (620 and 1055 Oe respectively), reflecting the high crystalline anisotropy of pyrrhotite, and H_R/H_c = 1.7, a reasonable SD value.

Day, Fuller & Schmidt (1977) have shown that J_{rs}/J_s and H_R/H_c are inversely correlated for sized synthetic titanomagnetites. The same general correlation holds for our samples (Fig. 6) but different groups of samples have different correlation constants. Most Leg 37 and 45 serpentinized samples fall on a single (PSD) curve, the Leg 37 rocks at the finer-size (or larger J_{rs}/J_s) end and the Leg 45 rocks at the coarser-size end, with considerable overlap. Leg 30 rocks, even those at the chilled margin, fall in a distinct low-J_{rs}, high-H_R/H_c group, transitional from large PSD to truly MD magnetite. The Leg 37 cumulate gabbros fall on a curve displaced from the curves for other samples, since their large J_{rs}/J_s values are those of fine PSD magnetite but their intermediate H_R/H_c values resemble those of much coarser PSD grains.

The results of Fig. 6 demonstrate that J_{rs}/J_s has a broad spread of values, from 0.05 to 0.5 for magnetite, that allows grain size within the PSD range (0.05–15 μm in magnetite) to

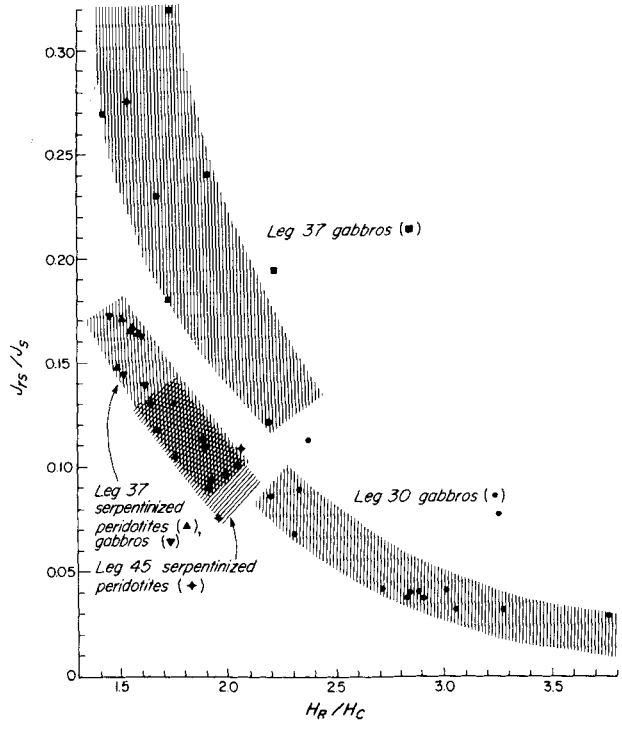

Figure 6. Inverse correlation of J_{rs}/J_s and H_R/H_c for submarine intrusive rocks, illustrating the lack of a universal correlation constant.

be determined with some assurance. But to judge from Fig. 6, H_R/H_c is less diagnostic, since H_R/H_c values in the narrow range 1.5–2.5 seem to characterize magnetite throughout the PSD range.

3.5 ALTERNATING-FIELD CHARACTERISTICS

Lowrie & Fuller (1971) proposed a test of domain structure based on alternating field (af) demagnetization characteristics of nrm or weak field trm (thermoremanent magnetization) and strong field irm (isothermal remanence). Nrm or trm softer than saturation remanence is an MD result; nrm or trm harder than saturation remanence is an SD result. Dunlop, Hanes & Buchan (1973) and Johnson, Lowrie & Kent (1975) subsequently showed that weak field arm (anhysteretic remanence) could substitute for trm and that PSD grains of magnetite gave an SD rather than an MD result of the test. Bailey (1975) pinpointed the changeover in test results: it occurs at the PSD–MD transition, around 15 μm in magnetite.

Af demagnetization of nrm, arm produced in a 1–Oe direct field and a 1.6 kOe rms af, and saturation (5 kOe) irm was carried out for five representative samples, one from each class of rocks, using a solenoid producing afs $\leq$ 1.6 kOe rms (2.25 kOe peak), a 3-axis tumbler and a Helmholtz coil field-free enclosure. Examples of the normalized intensity decay curves are given in Fig. 7 and the Lowrie-Fuller test results are summarized in Table 5.

Leg 30 gabbro 286–38–3a has soft, exponential-type af decay curves and an MD test result for both arm and nrm. Leg 37 unaltered gabbro 334–22–1c has extremely hard nrm and arm decay curves and an SD-like test result for both. However the nrm incorporates a much larger fraction of very hard grains than the arm.

Results for the three Leg 37 and 45 serpentinized rocks tested were less clear-cut. Serpentinized peridotite 334–22–2c (Fig. 7), for example, has relatively soft decay curves, but these are initially convex upward, like SD curves. The test result is MD for nrm but decidedly SD or PSD for arm. Arm and nrm are carried by different magnetite fractions, or perhaps both are carried by primary and secondary magnetite but in different proportions. It is also

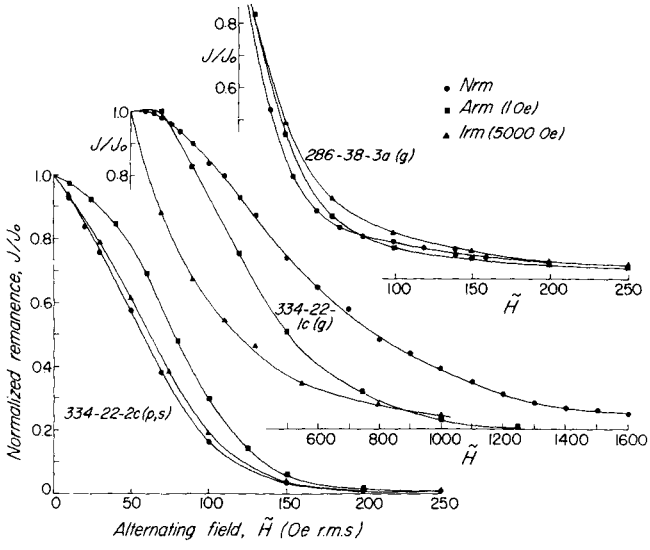

Figure 7. Comparison of normalized af intensity demagnetization curves of strong-field and weak-field remanences. Results can be classified as MD-like for 286–38–3a, SD-like for 334–22–1c and ambiguous for 334–22–2c.

entirely possible that although arm has a similar coercivity spectrum to nrm of trm origin, the same does not hold true for nrm originating as crm. The decay curves for 334–24–3b and 395–18–1a are ambiguous in a different way, giving an SD or PSD result for both nrm and arm at low afs and an MD result at higher afs. Bailey (1975) documented crossovers of this type in synthetic 2–15 μm magnetites.

3.6 DISCUSSION AND SUMMARY

Our strong-field isothermal magnetization and demagnetization experiments indicate that the primary magnetite in the Leg 30 doleritic gabbros, a product of exsolution subdivision of originally homogeneous large titanomagnetite grains, preserves a relatively coarse effective grain size. J_{rs}/J_s, H_R/H_c and Lowrie–Fuller results are definitely MD, demonstrating a grain size $\gtrsim 15\,\mu$m. The magnetite is abundant. It forms ≈ 1 per cent by volume or ≈ 2 per cent by weight of the rock. We anticipate that Layer 2B sills, *in situ,* are a potential source of surface magnetic anomalies, although the magnetization is rather soft and could be partially overprinted by later fields (this possibility will be tested in Section 4.1).

The primary magnetites present in Leg 37 gabbros as inclusions in silicates are predominantly $\lesssim 0.1\,\mu$m in size. J_{rs}/J_s values are $\gtrsim 0.3$ and the Lowrie–Fuller test result for 334–22–1c is unmistakably SD. Because of their ultrafine size, these magnetites are extremely hard ($H_R \gtrsim 300$ Oe, $\hat{H}_{1/2}$ for nrm from 450 to 750 Oe). However they form < 0.01 per cent by volume of the rock and impart a susceptibility comparable to that of the paramagnetic minerals. Fresh Layer-3 cumulate gabbros containing no secondary magnetite cannot be taken seriously as an anomaly source.

Some Leg 37 and 45 serpentinized gabbros and peridotites contain as much as 2.5 per cent by volume (or 5 per cent by weight) of secondary magnetite. Others are virtually paramagnetic, containing, in the case of the gabbros, only primary magnetite in pyroxenes or, in the case of peridotites, essentially no magnetite at all. There is no clear evidence from our collection that the production of secondary magnetite is simply correlated with degree of serpentinization.

The grain size of the secondary magnetite formed during serpentinization is also quite variable. In all cases, PSD behaviour is diagnosed but the secondary magnetites in Leg 37 cumulate rocks tend to be $< 1\,\mu$m in size, while those in Leg 45 upper-mantle peridotites tend to be $> 1\,\mu$m in size. The main evidence for the size ranges quoted is J_{rs}/J_s. Neither H_R/H_c nor the Lowrie–Fuller test is particularly helpful in discriminating between large and small PSD grains.

Strongly magnetic serpentinized rocks are candidates for a deep source (Layers 3 or 4) for oceanic magnetic anomalies, provided serpentinization of our samples occurred at depth and not following their later emplacement near the surface. Not only depth but also timing of the serpentinization is critical. Unless hydrothermal solutions percolate to lower crustal depths within, say 0.5 Ma of the time the magma cools through 600°C and acquires trm, the crm resulting from serpentinization will record a significantly later geomagnetic field than the primary trm. Cooling fronts are of course never vertical, but there are limits to the permissible time lag between near-surface and at-depth magnetic recordings at a given location if the integrated signal due to both sources is to yield a coherent stripe pattern at the ocean surface.

4 Natural remanent magnetization

Forty-five of our samples were oriented with respect to vertical, although none were

oriented in azimuth. In this section, we describe the stability of nrm directions in individual samples and the coherence of nrm inclinations among samples of a single unit. All magnetization measurements were made with a large-sample spinner magnetometer (Thellier 1967), which could accommodate the irregular shapes of our samples. Af demagnetization was accomplished with the solenoid and tumbler described in Section 3.5.

4.1 STORAGE TEST RESULTS

The capacity of the samples for viscous remagnetization was examined in storage tests lasting six weeks to three months. All 50 samples were stored three weeks with their vertical axes (or nominally vertical axes for the unoriented samples) parallel to the geomagnetic field and a further three weeks with their vertical axes antiparallel to the field. Subtraction of the nrms measured after the two storages yields approximately the vrm (viscous remanence) acquired on a 3-week time-scale. Addition of the results yields the nrm, approximately free of viscous contamination on this time-scale (although not necessarily free of vrm on a time-scale of years acquired in the DSDP core storage shed or vrm on a scale of ≈ 1 Ma acquired *in situ* in the oceanic crust).

Short-term vrm is negligible ($\lesssim$ a few per cent of the nrm) in all rock types except the Leg 30 doleritic gabbros (Fig. 8). The coarse MD magnetite grains in the Leg 30 samples range from moderately viscous (vrm $\approx 1-10$ per cent of nrm, seven samples) to exceedingly viscous (vrm $\approx 15-40$ per cent of nrm, eight samples) on a 3-week time-scale. The nrm of the more viscous samples is presumably largely or totally vrm acquired during the Brunhes epoch.

A second pair of storage tests was conducted after the nrms of 21 representative samples from all units had been reduced to very low levels by af demagnetization (Section 4.2). Large differences between viscosity coefficients measured before and after demagnetizing the nrm were reported by Lowrie & Kent (1978) for some oceanic basalts. Our intrusive rocks did not exhibit such large changes. However, if we disregard the weakly viscous samples, whose J_{vrm}/J_{nrm} ratios have large uncertainties, we observe that vrm acquired after af demagnetization is systematically about 25 per cent less than vrm acquired in the presence of the nrm.

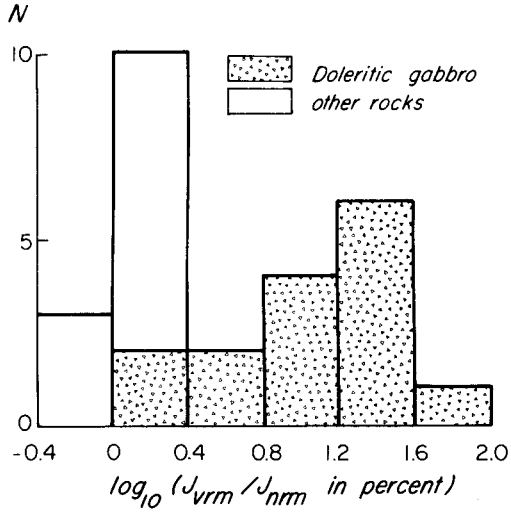

Figure 8. Histogram of viscosity indices, based on 6-week storage of undemagnetized samples in the Earth's field (note the logarithmic scale). Only the doleritic gabbros are strongly viscous.

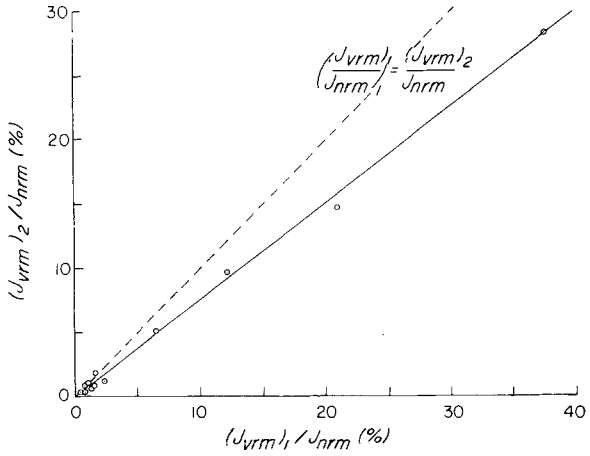

Figure 9. Comparison of viscosity indices before and after af demagnetization of nrm. The strongly viscous samples tend to become about 25 per cent less viscous after af cleaning.

4.2 AF CLEANING: ISOLATING SECONDARY NRMS

Secondary nrms acquired long after a rock's formation can be selectively erased and the primary nrm (trm or tcrm, and/or crm of secondary magnetite generated *soon* after cooling) enhanced by stepwise af demagnetization, if the secondary remanence(s) are softer than the primary nrm. The post-storage nrm in 21 of our samples, generally the more magnetic ones, was af demagnetized in steps to 1.6 kOe rms or until the remanence was less than 1 per cent of the initial nrm. Remanence directions in the course of af cleaning are plotted stereographically in Fig. 10.

All samples showed evidence of an underlying stable magnetization, often very different in direction from the initial nrm. Almost all unserpentinized samples and some serpentinized ones approached a stable endpoint direction before the nrm intensity fell below the noise level of the magnetometer.

There are a number of examples of three-component nrms in serpentinized rocks, e.g. 334–24–3b, 334–26–1a, 395–18–1d. In these examples, the intersection of two great-circle traces (remagnetization circles, Halls 1976), analogous to those in Fig. 10 but defined instead by difference vectors between nrms at adjacent cleaning steps, determines the direction of the remanence component of intermediate coercivity (Hoffman & Day 1978). In some cases, the intermediate-coercivity nrm may be crm of secondary magnetite formed during serpentinization and the high-coercivity nrm may be trm of primary magnetite. If so, the time lag between the remanences must have been considerable.

In sample 395–18–1d, the intermediate-coercivity nrm is likely akin to the steep initial remanences of other Leg 45 samples. Leg 45 intrusives are uniformly contaminated by a spurious near-vertical drilling remanence resulting from the use of a magnetic drilling collar during the ocean-bottom coring operation (H. P. Johnson 1978, private communication). The anomalous upward direction of this nrm component in 395–18–1d probably means that a section of core 18–1 was accidentally inverted.

All samples except the unaltered Leg 37 gabbros exhibit a low-coercivity nrm. The directions of both soft and hard components can, in favourable circumstances, be obtained from Zijderveld (1967) vector diagrams, like those of Fig. 11. The curves plotted are vertical- and horizontal-plane projections of the changing nrm vector. Segments of constant slope indicate that the vector being subtracted in the course of af cleaning has a constant direction, which

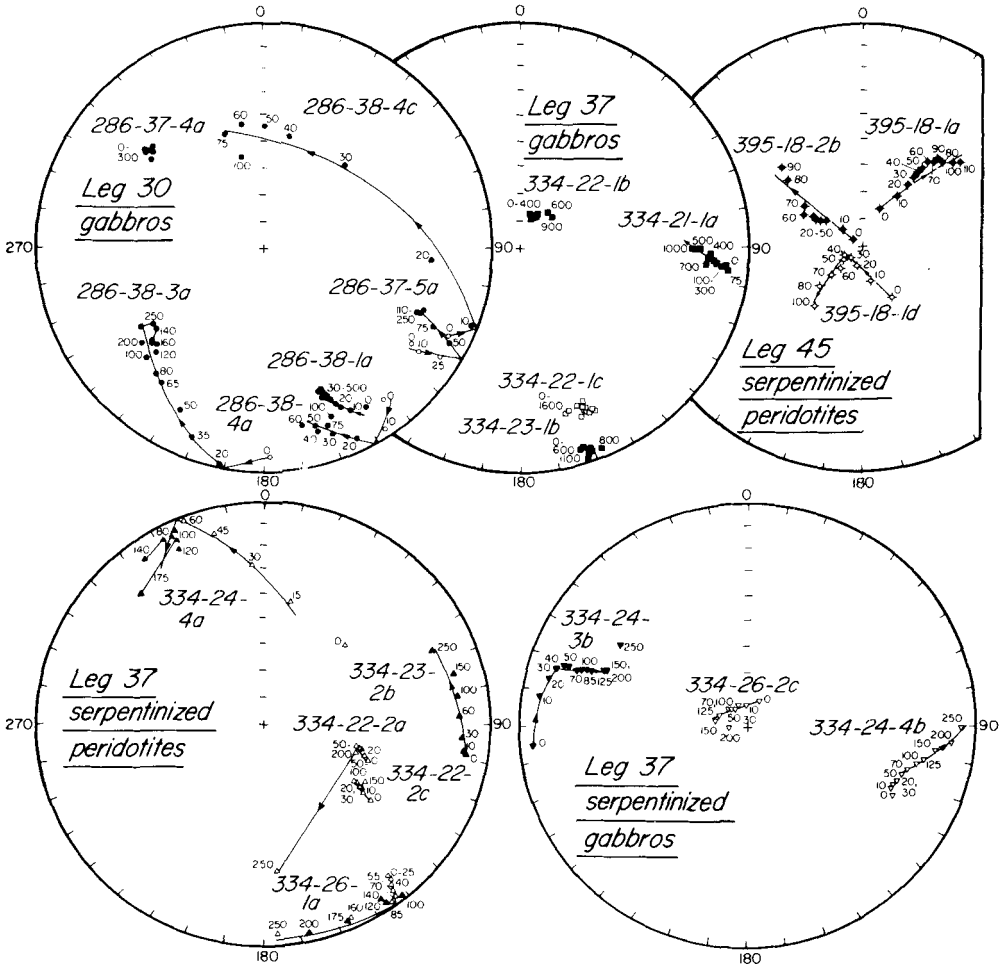

Figure 10. Equal area projections of nrm vectors in the course of af demagnetization. Numbers refer to the af applied in Oe rms. Stable endpoint directions are approached or reached in practically all samples. Only the viscous Leg 30 gabbros have large soft components of nrm.

can be determined from the slopes of the linear segments (e.g. Dunlop 1979). Linear segments that intersect the origin at high afs yield the stable end-point nrm direction, seen also in stereoplots. Linear segments at low afs yield the direction of the soft nrm component. The Zijderveld plots for our collection (Fig. 11) vary from ideal (e.g. 286–37–5a), with distinct linear segments defining both hard and soft nrm directions, to non-ideal, continuous curves (e.g. 334–24–4a) that express almost complete overlap of the coercivity spectra of the component nrms.

The soft nrms tend to have a common declination (relative to the arbitrary azimuth assigned the samples after their arrival at St Maur) and an inclination averaging $-30°$. The origin of these remanences is unclear. Their common declination rules out a secondary nrm acquired before the samples reached St Maur, whether of viscous origin or related to coring or sawing. On the other hand, a vrm produced by the second storage test (Section 4.1) would have an inclination of $-90°$ and in any case many of the samples were shown to acquire negligible vrm during the storage test.

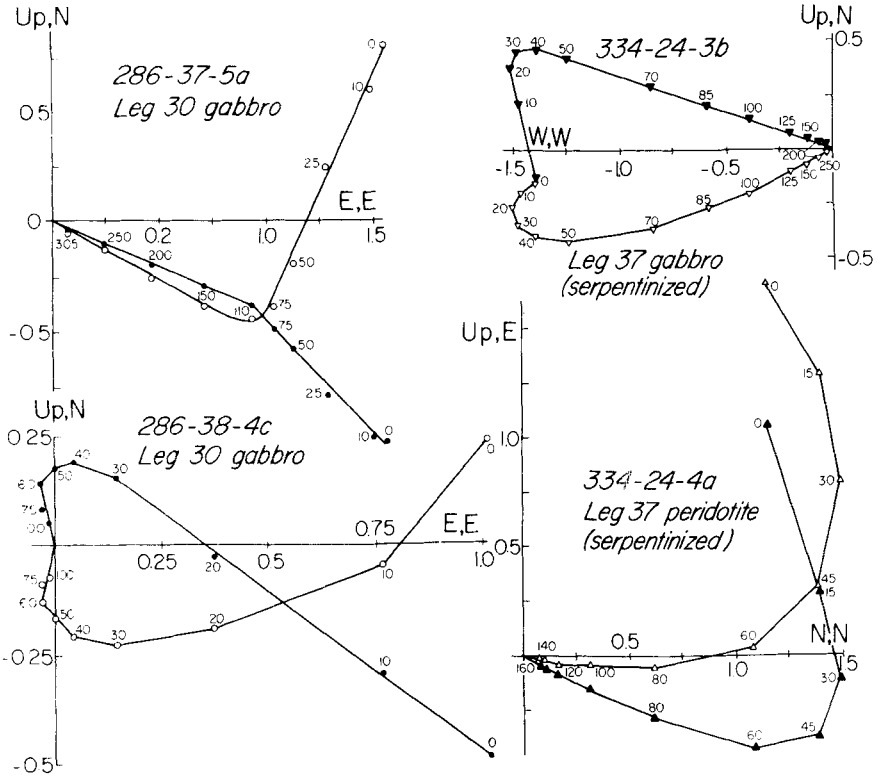

Figure 11. Vertical-plane (open symbols) and horizontal-plane (closed symbols) projections of nrm vectors in the course of af cleaning. Numbers are afs in Oe rms.

4.3 AF CLEANING: PRIMARY NRM DIRECTIONS

The primary nrm direction was taken to be the stable endpoint reached by the nrm vector during af demagnetization (Fig. 10) or, equivalently, the direction given by linear segments of the Zijderveld diagram at high afs (Fig. 11). Table 6 lists nrm inclinations, initially (before storage tests) and following optimum af cleaning, for the 15 samples that reached stable endpoints. Initial inclinations are also listed for samples from units 1, 2 and 3 of hole 334 (*cf.* Table 1) that were not af cleaned, because cleaned samples from these units exhibited single-component nrms uncontaminated by soft overprints.

Bracketed non-endpoint inclinations are given for three Leg 45 samples cleaned to $\lesssim 1$ per cent of initial nrm intensity to indicate the consistent swings to lower inclinations as the steep drilling remanence is erased. Although the drilling remanence is soft, it is so intense compared to the underlying stable nrm that we failed to isolate the primary direction. Evidently the stable nrm must have $I \lesssim +40^\circ$ (assuming that sample 395–18–1d is inverted). The dipole field inclination for this site latitude (23° N) is in fact about $\pm 40^\circ$.

Despite their striking propensity for viscous remagnetization, all six Leg 30 samples tested (some of them with short-term vrm/nrm ratios of 10–30 per cent) were successfully cleaned. Although vrm acquired over the Brunhes epoch might be expected to be more resistant to cleaning than short-term vrm, both types of vrm were apparently removed in comparatively small afs. The initially dispersed inclinations show a reasonable coherence after cleaning, with a mean of about $+32^\circ$. If the three most viscous samples (286–37–5a, 38–4a and

Table 6. Inclination and intensity of magnetization before and after optimum af cleaning of the nrm.

Sample no.	Inclination, $I(^\circ)$		Intensity, $J \times 10^3$ (emu cm^{-3})	
	Uncleaned	Cleaned	Uncleaned	Cleaned
Leg 30 doleritic gabbros				
286–37–4a	+ 34.6	+ 33.7	7.15	7.15
286–37–5a	– 6.4	+ 26.6	1.35	0.75
286–38–1a	+ 17.3	+ 31.2	5.5	$\geqslant$ 2.75
286–38–3a	– 1.9	+ 34.6	2.5	$\geqslant$ 0.3
286–38–4a	+ 2.0	+ 18.9	1.5	$\geqslant$ 0.65
286–38–4c	+ 19.6	+ 45.0	1.0	$\geqslant$ 0.25
Leg 37 cumulate gabbros				
334–21–1a	+ 9.8	+ 18.6	0.16	$\geqslant$ 0.125
334–21–1b	– 33.9		0.06	
334–21–1d	– 51.9		0.10	
334–21–1e	+ 51.0		0.15	
334–22–1a	+ 25.3		0.20	
334–22–1b	+ 78.8	+ 76.9	0.22	0.22
334–22–1c	– 21.7	– 22.6	0.53	0.53
334–23–1a	+ 56.6		0.03	
334–23–1b	+ 11.9	+ 3.8	0.14	0.14
Leg 37 serpentinized cumulate gabbros				
334–24–3b	+ 6.3	+ 30.0	0.79	$\geqslant$ 0.54
334–26–2c	– 82.0	– 81.1	0.74	$\geqslant$ 0.58
Leg 37 serpentinized cumulate peridotites				
334–22–2a	– 48.4	– 53.9	3.85	$\geqslant$ 3.1
334–22–2b	– 57.0		3.4	
334–22–2c	– 39.9	– 48.4	6.2	$\geqslant$ 5.2
334–24–4a	– 47.7	+ 8.0	1.25	$\geqslant$ 0.37
Leg 45 serpentinized peridotites (lherzolites)				
395–18–1a	+ 76.1	(+ 42.7)	8.2	> 0.12
395–18–1d	– 68.9	(– 62.7)	3.25	> 0.03
395–18–2b	+ 85.6	(+ 47.7)	11.4	> 0.06

38–4c) are excluded from the average, $\bar{I}$ is +33.2° with small dispersion about the mean. The dipole field inclination for this site latitude (16° S) is ± 30°.

Nrm vectors for most Leg 37 gabbros, whether fresh or moderately serpentinized, are individually quite stable but stable inclinations vary enormously from sample to sample. Since these rocks form part of an intrusive mélange, tectonic rotations are probably the cause of the scatter in primary (pre-emplacement) nrms.

The intensely magnetized Leg 37 serpentinized peridotites of unit 2, on the other hand, have reasonably coherent stable nrm directions. Averaging cleaned results for 334–22–2a and 2c and the uncleaned nrm of 22–2b, $\bar{I} \approx -53°$. The dipole field inclination for this site latitude (37° N) is ±58°.

4.4 NRM INTENSITY AND KOENIGSBERGER RATIO Q_n

Histograms of (uncleaned) nrm intensity (Fig. 12) show much the same pattern for the various rock types as that revealed by J_s and k_{fm} (Table 4), except that seven of the nine Leg 45 samples have disproportionately high nrm intensities attributable to drilling remanence. It is immediately clear from Fig. 12 that Layer 3 cumulate gabbros, whether fresh or

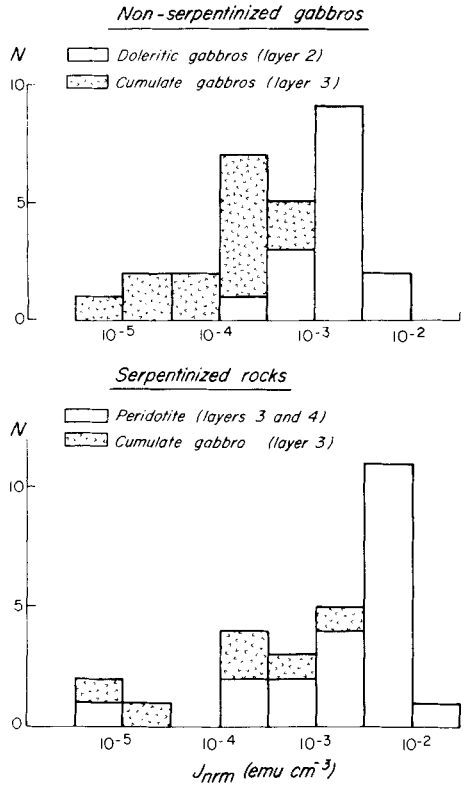

Figure 12. Histogram of nrm intensities (before cleaning). Doleritic gabbros and serpentinized peridotites are sufficiently intensely magnetized to rival pillow basalts as anomaly sources.

altered, can be disregarded as a potential source of magnetic stripes. Their nrm intensities are uniformly $\lesssim 10^{-3}$ emu cm^{-3}. Some serpentinized Layer 3 cumulate peridotites are sufficiently intense to deserve further consideration, with stable nrms ranging from 2.5 to 6×10^{-3} emu cm^{-3}.

In evaluating the Leg 30 and 45 rocks, it must be kept in mind that soft secondary nrm components account for part of the measured nrm intensity but only the stable nrm contributes to oceanic anomalies. If the Zijderveld diagram is ideal, intensities and af decay curves can be determined for the hard and soft nrm components separately (Zijderveld 1975; Dunlop 1979). This was a practical proposition for a few Leg 30 samples (*cf.* Fig. 11) but not for Leg 45 samples. Generally the cleaned nrm intensities given in Table 6 are total intensities at an af level sufficient to erase practically all soft nrm. They are therefore minimum estimates of intensity of the 'hard' nrm component, which itself usually has a low-coercivity fraction.

Layer 2B samples from the chilled margin of the Leg 30 doleritic sill have significant primary nrms, ranging from about 1.5 to 7×10^{-3} emu cm^{-3}. Interior samples, with similar ferrimagnetic contents but coarser grains, have probably insignificant stable nrms $\lesssim 10^{-3}$ emu cm^{-3}.

Leg 45 altered lherzolites are difficult to evaluate because drilling remanence almost totally obscures primary nrm, but it is safe to say that these rocks possess no nrm of significant intensity that is not magnetically very soft. Thus serpentinized upper-mantle peridotites do not seem to be prime candidates for a deep magnetic source.

The Koenigsberger ratio, Q_n, between nrm and magnetization induced by the present Earth's field (≈ 0.5 Oe) is a widely used measure of domain structure. We calculated Q_n values representative of the ferrimagnetic minerals only by excluding the paramagnetic induced magnetization of our weakly magnetic rocks. Q_n correlates rather well with the other measures of domain structure in Table 5. Interior samples from the Leg 30 sill (286–38–3a, 4a and 4c) have $Q_n \lesssim 1$, as expected for MD magnetite (Parry 1965, Stacey 1967). PSD grains in the Leg 30 chilled margin and Leg 37 samples have $1 \lesssim Q_n \lesssim 10$, the nearly SD grains of the fresh cumulate gabbros having the largest values. Q_n values for the Leg 45 rocks are anomalously high as a result of drilling remanence.

4.5 AF INTENSITY DECAY CURVES AND MEDIAN DESTRUCTIVE FIELD $\tilde{H}_{1/2}$

Normalized af intensity decay curves (Fig. 13) highlight the contrast between the very hard behaviour of the SD and small PSD primary magnetite inclusions in unaltered Leg 37 cumulate gabbros and the rather soft PSD and MD behaviour of primary and secondary magnetites in all other rock types. About 5 per cent of the nrm of cumulate gabbro 334–22–1c has coercivities in excess of 2250 Oe (peak) and must reside either in SD needles of magnetite or in SD pyrrhotite.

Values of the median destructive field (mdf), $\tilde{H}_{1/2}$, of nrm are tabulated in Table 5 for the 21 samples that were af demagnetized. Since the af decay curve could not usually be decomposed into separate decay curves for soft and hard nrm components, the mdf refers to the composite nrm. Table 5 and Fig. 14 demonstrate that for the very hard Leg 37 cumulate gabbros, remanent coercive force H_R is a reasonably close estimate of the mdf of nrm while

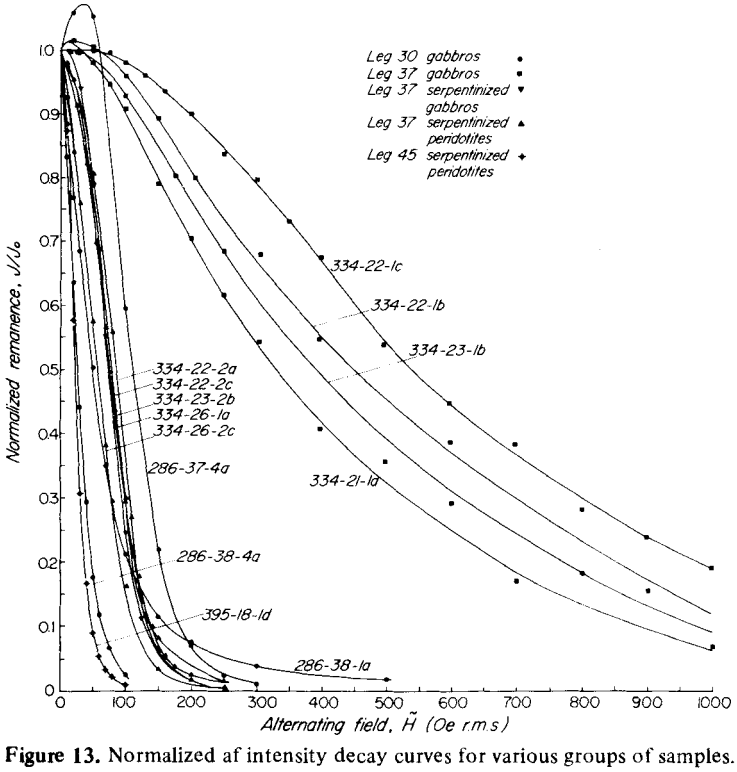

Figure 13. Normalized af intensity decay curves for various groups of samples.

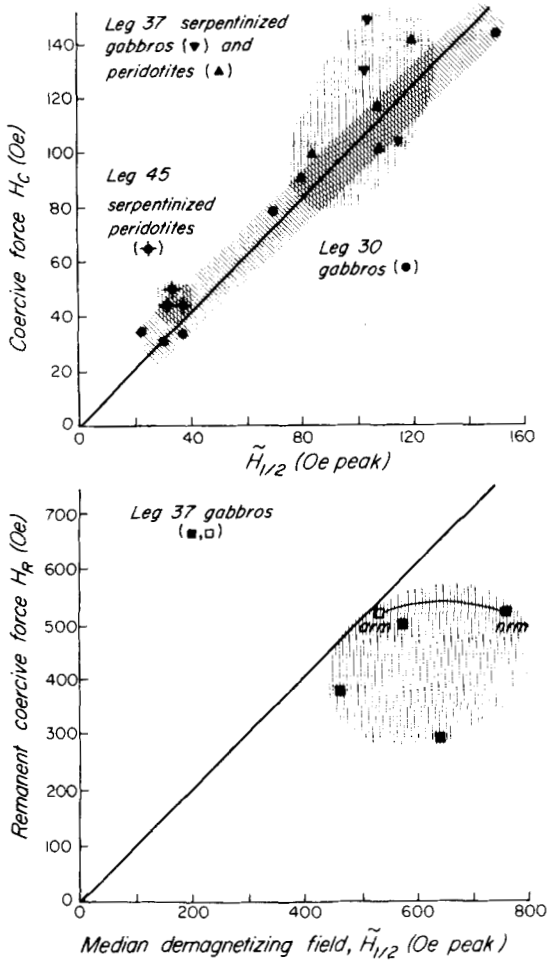

Figure 14. Correlations between median destructive field $\tilde{H}_{1/2}$ of nrm and either coercive force H_c (above PSD or MD carriers) or remanent coercive force H_R (below, SD magnetite).

coercive force H_c is a poor estimate. For the other rock types, the reverse is true. Of course, if soft vrm is an important component of the nrm, the mdf will tend to be lower than remanent coercivity from a rapidly determined hysteresis loop. This bias is insufficient to explain the effect evident in Fig. 14, however, particularly since only the Leg 30 rocks are strongly viscous. There is a real tendency for SD and nearly SD carriers to have $H_R \approx \tilde{H}_{1/2}$ and for larger PSD and MD carriers to have $H_c \approx \tilde{H}_{1/2}$.

Although generally speaking $\tilde{H}_{1/2}$ correlates with Q_n (Fig. 15), the different groups of samples behave in different fashions. Among Leg 30 gabbros, over a very broad size range from MD ($\geqslant 15\,\mu$m) to quite fine PSD ($< 0.5\,\mu$m), Q_n and $\tilde{H}_{1/2}$ have a simple power-law proportionality. The Leg 37 unaltered gabbros obey a similar but more complex relation (the exact relation is uncertain because Q_n is not very well determined for these weakly magnetic rocks). Leg 37 serpentinized rocks have a range of Q_ns but virtually constant $\tilde{H}_{1/2}$. Most of the Q_ns are lower than expected for intermediate-size PSD grains. The anomalous group of points for the Leg 45 rocks results from their spuriously high Q_n values (Section 4.4).

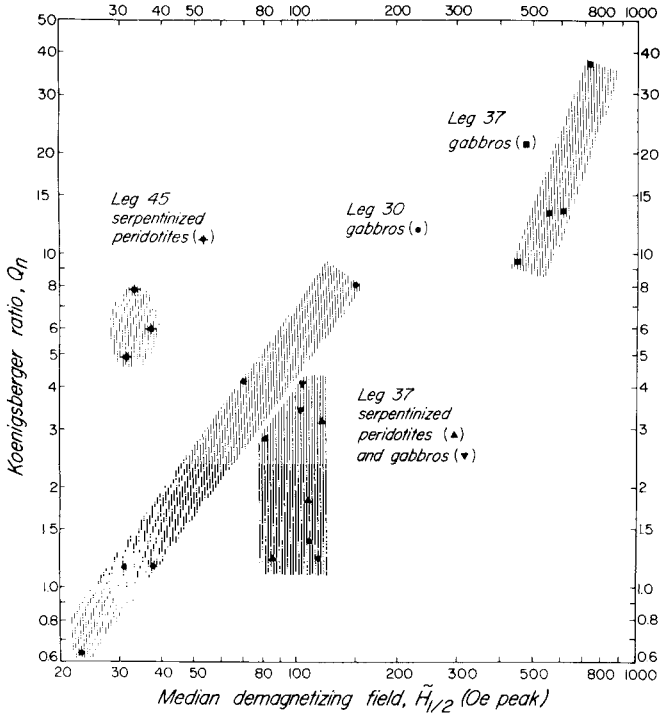

Figure 15. Classification of rock types by means of their correlation between Q_n and $\tilde{H}_{1/2}$. The Q_n values for Leg 45 rocks are spurious, since the nrm is overprinted by drilling remanence.

4.6 DISCUSSION

Samples from the Leg 30 doleritic sill have nrms $\geq 10^{-3}$ emu cm^{-3}, but the magnetizations of different samples do not agree in direction until soft viscous components of remanence (which would not contribute to stripe anomalies in the oceanic crust) have been erased by af demagnetization. Viscous components are unusually prominent in the coarse-grained sill interior. Storage tests indicate that up to 40 per cent of the nrm can reside in very short-term ($\approx$ 6 week) vrm. Zijderveld diagrams (Fig. 11) show that soft nrm (presumably incorporating longer-term vrm) is frequently comparable to (286–37–5c) or even exceeds (286–38–4c) stable nrm. (The storage-test vrm/nrm ratios for these samples were 12 and 38 per cent respectively.) However, the softer nrm component is easily erased, having maximum coercivities of $\approx$ 100 Oe rms for 37–5a and $\approx$ 60 Oe rms for 38–4c. There is almost no overlap with the coercivity spectrum of the stable nrm (100–300 Oe rms for 37–5a, 40–150 Oe rms for 38–4c), as is to be expected for purely viscous overprinting of a single type of magnetic carrier.

The stable nrm probably dates from initial cooling of the sill. It is oppositely directed to the present field at site 286 and has an average inclination close to the dipole field inclination at the site. The intensity of stable nrm ranges from $0.25–7 \times 10^{-3}$ emu cm^{-3}, being largest in the chilled margin where the magnetite grain size is finest. The Koenigsberger ratio Q_n is $\gtrsim 1$ for most samples, but when stable nrm only is considered, Q_n drops below 1 for samples from the sill interior. Only thin doleritic sills with substantial chilled margins are likely anomaly sources.

Layer 3 cumulate gabbros from Leg 37 are practically non-viscous and possess directionally stable nrms that have high Q_ns (≈ 10) and coercivities ($\bar{H}_{1/2} \approx 500$ Oe). Similar hard, stable behaviour has been reported for dredged gabbros (Irving *et al.* 1970; Fox & Opdyke 1973; Kent *et al.* 1978). However, whereas in some of these studies the gabbros possessed nrms $\approx 10^{-3}$ emu cm^{-3} in intensity, our collection was uniformly weakly magnetized, with arithmetic mean intensity 0.16×10^{-3} emu cm^{-3}. Moreover, the units sampled were incoherently magnetized, perhaps due to block rotations during emplacement. The fresh cumulate gabbros at site 334 are therefore not a possible anomaly source.

However, the serpentinized equivalents of these rocks are about three times more strongly magnetized and serpentinized peridotites in the same sequence are five times more magnetic still. Indeed serpentinized cumulate peridotites were the only rock type we examined that possessed all the requisites of a source of linear anomalies: arithmetic mean nrm intensity of 2.4×10^{-3} emu cm^{-3}; short-term vrm < a few per cent of nrm; $Q_n > 1$; $\bar{H}_{1/2} \gtrsim 100$ Oe, and a directionally stable and coherent component of nrm of ancient origin in samples from certain units. Samples 334–22–2a, 2b and 2c (unit 2), for example, have an average (cleaned) nrm inclination of $-53°$, close to the expected dipole inclination and opposite to the present field inclination.

This nrm is not primary trm, which would begin to block just below 580°C, but crm carried by secondary magnetite generated below 500°C during serpentinization. Because of slow cooling at depth, the time lag between intrusion and crm acquisition could be substantial even if serpentinization occurred in the lower crust rather than after emplacement. At site 334, basalts in the uppermost 60 m of the crust have positive inclinations, consistent with the normal polarity of the site anomaly. The negative inclinations of the underlying unit 2 peridotites may record a time lag in magnetization due to slower cooling at depth (non-vertical cooling front), an additional time delay before serpentinization began, and perhaps also lateral (as well as vertical) emplacement of the intrusive mélange.

The coherence of nrm inclinations in our three unit-2 peridotites is indirect evidence for the time of nrm acquisition. Since all the unserpentinized gabbros, which were emplaced in a similar manner, are incoherently magnetized, serpentinization and magnetization of this unit may have followed its emplacement near the surface. On the other hand, since serpentinization occurs principally above 250–300°C (e.g. Cann 1979), crm was presumably acquired at depth. Emplacement without significant rotation, or with tectonic discontinuities on a scale larger than the spacing of our samples, could have preserved the original spatial pattern of crm directions.

Leg 45 serpentinized lherzolites were contaminated by drilling remanence to such an extent that no firm conclusions can be drawn about their intrinsic nrms. They gave every indication of being very soft. After 100 Oe rms cleaning, the nrm direction approached the expected dipole inclination at site 395, but the intensity had dropped below 0.1×10^{-3} emu cm^{-3}, a level that is insignificant as far as anomaly production is concerned.

5 Discussion

5.1 COMPARISON WITH RESULTS OF OTHER STUDIES

Previous systematic studies of the intrusive layers of the oceanic crust have relied on obducted ophiolite suites or seafloor dredgehauls. Results of these studies are summarized in Table 7 and compared with our findings for drilled intrusives.

Such comparisons have value only if the magnetic properties of ophiolitic and dredged samples have not been degraded during and after their surface emplacement. A reasonable minimum criterion is that their metamorphic grade and magnetic mineralogy should match

Table 7. Comparison of magnetic properties of intrusive rocks from ophiolite suites and from seafloor dredging or drilling.

Location	Metamorphic grade	N	$\bar{J}_{nrm}$ (10^{-3} emu cm^{-3})	Direction of nrm	$\bar{Q}_n$	$\tilde{H}_{1/2}$	Vrm/Nrm (per cent)	T_c (°C)
Doleritic sills								
Othris, Greece★	Greenschist?	6	0.09[b]	Underlying stable	0.2	100–140	15–41[d]	570
DSDP Leg 30 (this study)	Zeolite	15	2.0[b]	Underlying stable	2.0	25–180	1–42[e]	530
Sheeted dykes								
Troodos, Cyprus†‡	Greenschist	40	1.3[a]	Underlying stable	≲1	100–200	31[c]	550
Macquarie Island‡	Amphibolite	32	0.02[a]	Stable	0.5	300–500	8[c]	580
Smartville, CA‡	Greenschist	122	0.13[a]	Unstable	0.8	<100	21[c]	565
Othris, Greece★	Greenschist?	14	0.19[b]	Underlying stable	0.4	50–220	10–76[d]	570
Gabbros								
Troodos, Cyprus†		49	≈1[a]	Stable	≈10			
Macquarie Island§		18	0.2[a]		0.6			
Smartville, CA§	Greenschist?	24	0.3[a]		1.1			
Othris, Greece	Amphibolite?	8	0.01[b]	Stable	0.5			540
Vourinos, Greece§	Amphibolite?	91	0.03[a]		1.2			
Samail, Oman¶		67	0.9		5			
Mid-Atlantic Ridge, 45° N★★††‡‡		8	0.23[b]	Stable	(≈15)	385–500		200–300, 525–540
Atlantic FZ's§§¶¶	Mixed	69	0.88[b]	Stable	8	50–800		575
Mid-Cayman Rise★★★		≈50	0.48	Stable	1.6	50–800		535–580
DSDP Leg 37 (this study)								
(1) Unaltered	Fresh	10	0.16[b]	Stable	12.7	467–765	⩽3[e]	560
(2) Serpentinized		6	0.48[b]	Stable	2.5	105–115	⩽2[e]	570
Serpentinized peridotites								
Troodos, Cyprus† Pyroxenite, dunite		29	≈7[a]	Underlying stable	≈10			
Othris, Greece★ Lherzolite		9	2.9[b]	Unstable	9.5	70–90	⩽4[d]	565
Mid-Atlantic Ridge 45° N★★‡‡		5	3.2[b]	Stable	22	265–385		
Kane FZ§§		3	8.2[b]	Stable	2.5	≈100		
DSDP Leg 37 (this study) Cumulate peridotite		10	2.4[b]	Stable	2.0	80–120	⩽3[e]	565
DSDP Leg 45 (this study) Lherzolite		9	(5.5)[b]	Underlying stable?	(4.8)	(30–40)	⩽3[e]	570

Notes:
[a] Geometric mean.
[b] Arithmetic mean.
[c] Vrm projected to 0.7 Ma.
[d] Vrm acquired in 10 week.
[e] Vrm acquired in 6 week.

References:
★ Beske-Diehl & Banerjee (1979).
† Vine & Moores (1972).
‡ Levi & Banerjee (1977).
§ Banerjee (1980).
¶ Day & Luyendyk (1979).
★★ Irving *et al.* (1970).
†† Carmichael (1970).
‡‡ Park & Irving (1970).
§§ Fox & Opdyke (1973).
¶¶ Kent *et al.* (1978)
★★★ Caytrough (1979).

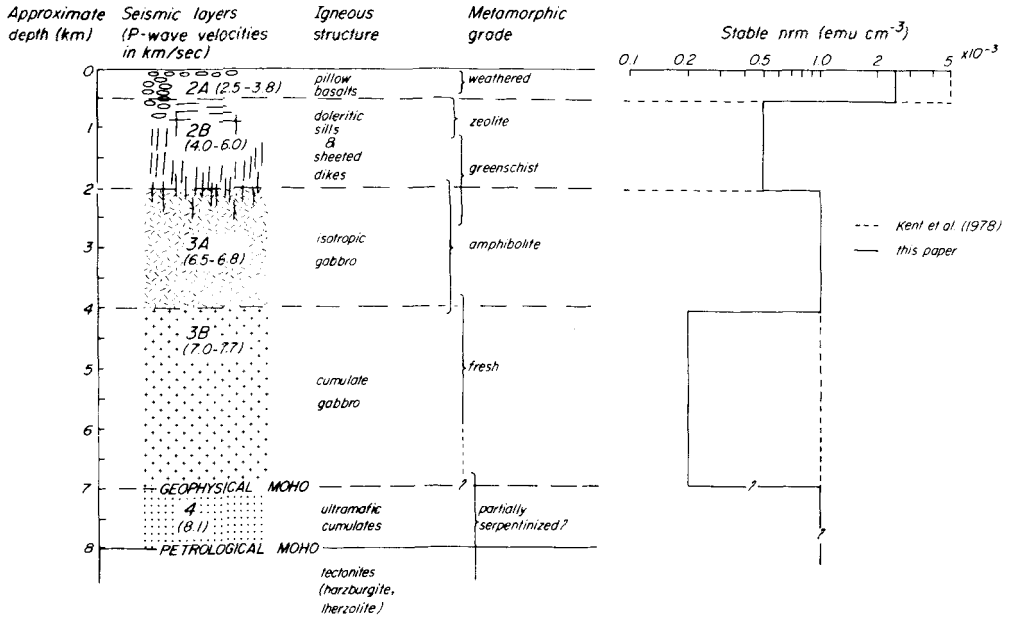

Figure 16. The lithologic, seismic and metamorphic zonation of the oceanic crust, with the corresponding magnetic layering suggested by Kent *et al.* (1978) and by us. Our model and Kent *et al.*'s differ principally in the stable nrm intensities assigned to Layers 2B and 3B. In either case, intrusive and plutonic rocks constitute one-half or more of the source of oceanic magnetic anomalies. (Seismic layers after Peterson *et al.* 1974, Christensen & Salisbury 1975 and Stern *et al.* 1976. Igneous structure from Stern *et al.* 1976 for the upper crust and Dewey & Kidd 1977 for the lower crust. Metamorphic zones for the upper crust after Stern *et al.* 1976.)

that observed or inferred for oceanic crust at a corresponding stratigraphic level (Levi *et al.* 1978; Banerjee 1980). Such a test can only be applied directly to the extrusive rocks, since only Layer 2A has been drilled by DSDP. The stratigraphic and metamorphic succession in the deeper crust is deduced in large part from that of ophiolites.

Fig. 16 shows the primary igneous 'pseudostratigraphy' and seismic zonation proposed by Stern, deWit & Lawrence (1976). It is based specifically on the structure of Chilean ophiolites, but is in general accord with other models of crustal composition and metamorphic zonation (e.g. Cann 1968, 1974, 1979; Peterson, Fox & Schreiber 1974; Christensen & Salisbury 1975; Dewey & Kidd 1977). The top 5 km of the crust has a steep metamorphic gradient, passing from zeolite facies in Layer 2A to amphibolite facies in Layer 3A. It overlies relatively fresh gabbros and peridotites. The boundary between amphibolitized and underlying fresh gabbro probably corresponds to the Layer 3A–3B boundary (Fox, Schreiber & Peterson 1973; Christensen & Salisbury 1975). The near-surface metamorphic gradient is attributed to hydrothermal and contact metamorphism associated with deep seawater circulation in faults close to and paralleling the mid-ocean ridge (Talwani, Windisch & Langseth 1971; Lister 1972).

Cann (1979) envisages three episodes of seawater convection. Initial faulting and convection occurs within the median valley after about 1 km of spreading has occurred and penetrates to the nearly molten zone capping the magma chamber (Fig. 1). Intense hydrothermal circulation cools the hot crust and rapidly establishes the high-temperature metamorphic zonation (zeolite-greenschist-amphibolite) with depth in the vicinity of the fault zone. After a hiatus, renewed convection follows extension of brittle fracturing into the lower crust and

upper mantle. The metamorphic mineral assemblage in the upper 5 km of the crust is little changed but the lower crust and upper mantle are serpentinized. Serpentinite diapirs subsequently penetrate into the upper crust, particularly in fracture zones. The final episode of convection is mild but prolonged. It extends low-temperature alteration (Cann's 'brownstone' facies to zeolite facies metamorphism) into the interior of fault blocks.

Judging by observed levels and zonation of metamorphism, few ophiolite complexes were sufficiently gently obducted to have remained good analogues of *in situ* oceanic crust. Because of the high metamorphic grade of the pillow lavas, Levi *et al.* (1978) rejected all but the Troodos and Macquarie Island ophiolites. The Troodos basalts pass from zeolite into greenschist facies, with an accompanying sharp increase in Curie point, at a subsurface depth of about 1.5 km (Beske-Diehl & Banerjee 1980). This zonation is as expected. The Macquarie Island ophiolite, however, should be rejected, since its sheeted dykes are in amphibolite rather than greenschist facies (Table 7). Rather than rejecting the bulk of ophiolitic data sight unseen, we have preferred to retain all the published data, but caution is clearly called for in drawing conclusions from the comparisons that follow.

A limited sampling (six samples, one site) of a doleritic sill from the Othris ophiolite (Beske-Diehl & Banerjee 1979) yields results that compare closely with those for our Leg 30 sill: Curie points are those of pure magnetite; coercivities are low and short-term vrm is high (up to 40 per cent of nrm); but the nrm has an underlying stable component revealed by af demagnetization. The main difference between the two studies is that our samples have an arithmetic mean nrm intensity $\bar{J}_{\mathrm{nrm}}$ of 2×10^{-3} emu cm^{-3} and $\bar{Q}_{\mathrm{n}} = 2$ while the Othris samples have $\bar{J}_{\mathrm{nrm}} \approx 0.1 \times 10^{-3}$ emu cm^{-3} and a correspondingly low $\bar{Q}_{\mathrm{n}}$. The low intensities of the Othris sill rocks probably result from their higher metamorphic grade (chlorite is present in the Othris samples but absent from all our samples).

Samples from the sheeted dyke complexes of the Othris and most other ophiolites (Levi & Banerjee 1977) have similarly low intensities but T_{c}, Q_{n}, $\tilde{H}_{1/2}$ and vrm/nrm values are much like those of fresh sills. The unaltered section of the Troodos sheeted dykes (Vine & Moores 1972), with $\bar{J}_{\mathrm{nrm}} = 1.3 \times 10^{-2}$ emu cm^{-3} (geometric mean), seems to be the sole ophiolitic analogue of fresh Layer 2B intrusives *in situ*.

Comparison of the magnetic properties of oceanic gabbros is complicated by the variety of metamorphic facies and petrological types represented (e.g. Kent *et al.* 1978, p. 517). Our relatively fresh cumulate gabbros have $\bar{J}_{\mathrm{nrm}} = 0.16 \times 10^{-3}$ emu cm^{-3}, rising to $\approx 0.5 \times 10^{-3}$ emu cm^{-3} if the gabbros have been serpentinized. These nrm intensities are consistent with those of most ophiolites and of dredged gabbros from the Mid-Atlantic Ridge and the Mid-Cayman Rise. [Some of the Mid-Cayman Rise rocks have been identified as cumulates (Caytrough 1979), like ours.] In contrast, gabbros from the Troodos and Samail ophiolites and from North Atlantic fracture zone dredgehauls (Kent *et al.* 1978) have $\bar{J}_{\mathrm{nrm}} \approx 10^{-3}$ emu cm^{-3}.

The more strongly magnetized fracture zone samples tend to be noritic gabbros, differentiates that probably crystallized out on the walls of the magma chamber (Cann 1974; see Fig. 1), and amphibolite-grade metagabbros containing secondary magnetite (Stern *et al.* 1976). Thus the average nrm intensity for the fracture zone dredgehauls should perhaps be taken as more representative of metamorphosed Layer 3A (Christensen & Salisbury 1975) and the top of Layer 3B and our values as more representative of the rest of Layer 3B. Whatever their nrm intensities, oceanic gabbros seem to be stably magnetized. The nrm resides in pure magnetite with $Q_{\mathrm{n}} \approx 1$–10 and $\tilde{H}_{1/2} \approx 50$–$800$ Oe.

Serpentinized peridotites have been rather sporadically recovered in earlier studies. Our 19 Leg 37 and Leg 45 samples represent almost a third of the total data base. It is therefore difficult to judge what results are typical. All studies agree that secondary magnetite is the key magnetic mineral, and that it is produced abundantly during serpentinization. Mean nrm

intensities are invariably high ($2.4–8.2 \times 10^{-3}$ emu cm^{-3}), although the stable fraction of nrm (the anomaly source) is extremely variable. The nrm tends to be soft ($\tilde{H}_{1/2} \approx 100$ Oe) but $\bar{Q}_n \geqslant 2$, and short-term vrm $\leqslant 4$ per cent of nrm. Despite these indications of reasonable stability, nrms of both ophiolites represented (Troodos and Othris) are either widely dispersed or substantially remagnetized in the direction of the present Earth's field. All seafloor samples, on the other hand, are either stably magnetized or possess an underlying stable component of nrm. (The directional fidelity of the nrm of the dredged rocks cannot of course be tested.)

5.2 PRIMARY MAGNETIC MINERALOGY OF OCEANIC INTRUSIVE ROCKS

The principal magnetic mineral in the doleritic sill sampled by Leg 30 is abundant titanomagnetite that has been deuterically oxidized at temperatures $\geqslant 600$°C to an exsolution intergrowth of ilmenite and low-titanium titanomagnetite. Layer 2A basalts contain titanomagnetite of similar bulk composition which has been preserved in a metastable homogeneous state by quenching from high temperature and subsequently maghemitized as a result of low-temperature oxidation by percolating sea-water.

The slower cooling of Layer-2B dykes and sills and ensuing high-temperature oxidation have three principal magnetic consequences.

(1) The oxide grain-size is very coarse. Even though grains are subdivided by ilmenite lamellae, their magnetic behaviour is MD (effective grain size $\gtrsim 15\,\mu$m). Their trm is therefore considerably less intense and stable than the trm of a similar quantity of fine SD or pseudo-SD magnetite in a rapidly chilled rock. Chilled margins of dykes and sills take on particular importance as a location of relatively hard and intense trm.

(2) Magnetite ($T_c = 580$°C), rather than titanomagnetite containing 60 mol per cent Ti ($T_c \approx 140$°C), is the magnetic carrier. The Curie point isotherm is therefore deep in the crust.

(3) The deuterically oxidized titanomagnetites are immune to later low-temperature oxidation. Thus the initially large contrast between the nrm intensities of Layer 2A and Layer 2B rocks is reduced considerably as the titanomagnetites in the extrusives are maghemitized (Irving *et al.* 1970; Johnson & Atwater 1977; Prévot *et al.* 1981).

In the fresh cumulate gabbros of Leg 37, the primary magnetic mineral is titanium-free magnetite present as infrequent fine ($\lesssim 1\,\mu$m) inclusions in pyroxene and plagioclase. Such a mode of occurrence is familiar from continental mafic plutonic rocks (e.g. Evans & Wayman 1970), which sometimes possess intense and stable nrms as a result. Since the inclusions are a product of deuteric oxidation at high temperatures (≈ 800°C), the nrm is a primary trm. The nrm is immune to chemical alterations because the inclusions are protected by their silicate hosts from hydrothermal solutions (*cf.* Banerjee, Butler & Stout 1974). The fine grain size results in SD or SD-like stability of the nrm. Unfortunately, these near-ideal characteristics are offset in our collection by the low abundance of magnetite inclusions (< 0.01 per cent by volume, Table 4), which results in nrm intensities $< 10^{-3}$ emu cm^{-3}. Submarine gabbros appear to be extremely variable in their magnetite contents, however (*cf.* Kent *et al.* 1978; Caytrough 1979) and our samples may not be typical.

5.3 EFFECT OF ALTERATION AND METAMORPHISM ON OPAQUE MINERALOGY AND MAGNETIC PROPERTIES

Our samples show the effects of low-temperature alteration (rims of silicates altered to clay minerals) and serpentinization of olivines but there is no evidence of metamorphism to

greenschist facies. Chlorite is absent and many gabbros are very fresh. Maghemitization, which is the principal consequence of low-temperature alteration of Layer 2A basalts at depths up to 0.6 km, is not seen in any of our intrusives, whatever their depth of origin. The primary magnetites in doleritic sills and cumulate gabbros are presumably immune because they have been previously oxidized deuterically or are protected by silicate hosts. The observation is more puzzling for the secondary magnetites, particularly since at site 334 the serpentinized rocks have been exposed to the same sea-water circulation as the adjacent highly maghemitized pillow basalts. The larger grain size of magnetite in the serpentinites may have served to minimize oxidation. In any case, inversion of titanomaghemite at $>300^{\circ}$C, proposed by Banerjee, Levi & Bogdan (1977) as a mechanism of magnetite generation, seems improbable in Layer 2B or Layer 3.

Greenschist- and amphibolite-facies metamorphism was not observed in our collection of gabbros. Fox & Opdyke (1973, table 3) and Kent *et al.* (1978, table 3) have reported comparable nrm intensities for fresh gabbros and for metagabbros. However, the development of secondary magnetite in Fox & Opdyke's amphibolites has been documented by Stern *et al.* (1976) and in Kent *et al.*'s collection, metagabbros and noritic gabbros (likely constituents of Layer 3A) tend to have larger nrms than the other rocks.

Serpentinization of olivines is a very frequent consequence of hydrothermal alteration of our gabbros and peridotites. The associated precipitation of secondary magnetite renders the peridotites strongly magnetic. The phase Ni_3Fe, which according to Lienert & Wasilewski (1979) is present in all serpentinites, was not observed in our rocks. In contrast to the generally unstable nrm of continental serpentinites (e.g. Saad 1969), the secondary magnetite in most of the serpentinized rocks we examined was of intermediate PSD size with $J_{rs}/J_s \approx 0.2$ and Q_n well above 1. As a result the nrm was in large part stable. Even higher stability has been observed for Mid-Atlantic Ridge serpentinites (Table 7).

5.4 TECTONIC EFFECTS

Rotation of fault blocks on the flanks of the axial rift zone has been invoked to account for scattered, generally non-dipole nrm inclinations in pillow basalts, particularly those from the three deep holes of Leg 37 (Hall 1976; Prévot *et al.* 1979). Among our samples, Leg 30 rocks definitely possess an unrotated primary nrm component and Leg 45 lherzolites have a weak underlying nrm whose direction approximates the expected dipole inclination. Block faulting would be expected to penetrate Layer 2B as well as Layer 2A, and the Leg 45 rocks originated at mantle depths and must have been fault-emplaced near the surface. Thus block faulting on a crustal scale is not invariably accompanied by block rotation.

The Leg 37, site 334 gabbros and peridotites for the most part possess individually stable but mutually inconsistent nrm orientations. The complex faulting that led to the gabbro-peridotite intrusive mélange may have resulted in large rotations on a rather local scale. However, unit 2 has consistent nrm inclinations close to the dipole value. In Section 4.6, this observation was cited as possible evidence that unit 2 was serpentinized and acquired crm after it was tectonically emplaced (the same could be argued of the Leg 45 lherzolites). It is not inconceivable that instead unit 2 was emplaced without significant rotation.

5.5 OCEANIC INTRUSIVE ROCKS AS AN ANOMALY SOURCE

There is mounting evidence that although pillow basalts of Layer 2A are the principal source of magnetic stripes, part of the source must lie deeper in the crust. Harrison (1976) has given an exhaustive survey of all the lines of evidence. Modelling anomaly amplitudes by crustal

blocks of uniform magnetization requires a 0.5 km thick layer with nrm intensity $\approx 10^{-2}$ emu cm^{-3} (Harrison 1976, table 2) or a thicker layer with the same product of J_{nrm} and thickness. Direct measurements of unmetamorphosed DSDP basalts (Lowrie 1974, 1977; Harrison 1976, table 4) give a mean J_{nrm} of $\approx 2.5 \times 10^{-3}$ emu cm^{-3}. Either Layer 2A is 2 km thick, which is ruled out by seismic evidence, or up to half the source is in Layer 2B or Layer 3.

Another approach is to determine the depth of the source from the power spectrum of the observed linear anomalies for an average reversal rate of 1.58 Ma^{-1}. Although many combinations of layer thickness and depth to the top of the source were permissible, the depth to the middle of the layer remained approximately constant at ≈ 6.8 km below the ocean surface (Harrison 1976, table 6).

Kent *et al.* (1978) have proposed a source consisting of 0.5 km of strongly magnetized pillow basalts and >3 km of metagabbro (Layer 3A) and fresh gabbro (Layer 3B) with average nrm intensity $J_{nrm} \approx 10^{-3}$ emu cm^{-3}. Layer 2B is taken to be weakly or unstably magnetized. The viability of their model rests on three assumptions:

(1) zeolite- and greenschist-facies metadiabases possess weak, unstable nrms;
(2) the whole of Layer 3 consists mainly of gabbro with $J_{nrm} \approx 10^{-3}$ emu cm^{-3};
(3) serpentinites are an unimportant constituent of Layer 3, except locally in fracture zones.

Greenschist-facies metavolcanics ('greenstones'), whether oceanic or continental, tend to be almost devoid of magnetic minerals (e.g. Fox *et al.* 1973) but metadiabases of similar grade preserve a reasonable fraction of their original nrm, presumably because the larger grains are more resistant to chloritization. Furthermore, doleritic sills in the shallower part of Layer 2B are in the zeolite facies. The sheeted dyke complex in the Troodos complex is by no means weakly magnetized; in fact, it is more strongly magnetized than the underlying gabbros (Table 7). It is true that a considerable fraction of nrm in the coarse-grained interiors of dykes and sills is soft and likely of viscous origin, but hard components with intensities $\gtrsim 0.5 \times 10^{-3}$ emu cm^{-3} were uncovered by af cleaning in our Leg 30 doleritic sill samples (Table 6). We believe rocks with this level of stable nrm may occur frequently in Layer 2B, and that Layer 2B should not be disregarded as a possible source.

Oceanic gabbros are so heterogeneous in their nrm intensities that it is futile to generalize. Average values refer to a mixture of metamorphic grades and petrological types that may or may not be characteristic of Layer 3. In our collection of 10 fresh cumulate gabbros, the maximum nrm was 0.5×10^{-3} emu cm^{-3} and most were in the range $0.1–0.2 \times 10^{-3}$ emu cm^{-3}. Only when the gabbros were serpentinized did the nrms rise to significant levels. On the other hand, gabbros dredged from Atlantic fracture zones (Kent *et al.* 1978) had $J_{nrm} \approx 1 \times 10^{-3}$ emu cm^{-3}. The most intensely magnetized of these rocks were noritic gabbros and amphibolite-grade metagabbros, probably originating in the upper part of Layer 3. Thus we tentatively propose that Layer 3A and uppermost Layer 3B have an average intensity of stable magnetization $\approx 1 \times 10^{-3}$ emu cm^{-3}, as proposed by Kent *et al.* (1978, fig. 10), but that the remainder of Layer 3B (fresh cumulate gabbro) has a much weaker average intensity, $\approx 0.2 \times 10^{-3}$ emu cm^{-3}. As a provisional value of J_{nrm} for Layer 3 as a whole, we propose a simple arithmetic mean of the gabbro J_{nrm} values in Table 7, namely $\approx 0.5 \times 10^{-3}$ emu cm^{-3}.

There seems to be no question that serpentinites possess a sufficiently intense stable nrm to compete with Layer 2 extrusive and intrusive basaltic rocks as an anomaly source. The real questions are how important a constituent of the oceanic crust serpentinites are and how soon after intrusion they acquire crm. Harrison (1976) has reviewed thoroughly the case for and against the widespread presence of serpentinized rocks in Layer 3. He points out

that the presence of about 20 per cent serpentinite might go undetected seismically but would be extremely important magnetically. We would simply note that, perhaps coincidentally, the two earliest deep-penetration legs of DSDP, 37 and 45, both recovered significant sections of serpentinized peridotites of deep origin (Layer 3B cumulates and upper-mantle lherzolites respectively).

Serpentinites are so much more intensely magnetized than other intrusive rocks ($J_{nrm} \approx 5 \times 10^{-3}$ emu cm^{-3}, Table 7) that their presence at either deep or shallow levels in the crust must have a decided magnetic anomaly signature. Whether that signature enhances the magnetic stripes or disrupts them depends on the timing of serpentinization and the directional coherence of the crm produced. Coherence of the crm, on a small scale at any rate, is demonstrated by the approximately dipole inclinations of cleaned nrm in two of our groups of samples, unit 2 peridotites at site 334 and site 395 lherzolites (Table 6). The time of crm acquisition is less certain. The reversely polarized crm of unit 2, which has a destructive effect on the net positive anomaly at site 334, must have been acquired $\gtrsim 0.5$ Ma after pillow lavas in the same sequence acquired primary trm. Self-reversed crm is unlikely since lherzolites at site 395 are normally polarized, reinforcing the net positive anomaly at this site. The site 395 peridotites may have been serpentinized within 0.5 Ma or so of formation or, alternatively, during a later positive polarity epoch.

A related question is the depth at which serpentinization occurred. Cann (1979) hypothesizes that serpentinization occurs at lower crustal and upper mantle depths, as soon as a significant temperature gradient is reestablished following initial (≈ 0.1 Ma) convection to the Layer 3A/3B boundary. On this model, Layer 3 and Layer 4 serpentinites could be widespread and would carry an early crm reinforcing the magnetic signal of Layer 2 basaltic pillows and dykes.

Serpentinization during or following tectonic emplacement at shallow depths, on the other hand, is as likely to disrupt magnetic anomalies as to reinforce them, since emplacement could lag one or more polarity epochs behind initial cooling. Serpentinization is probably not widespread near the surface because the minimum temperatures of 250–300°C required are encountered only at depths of several kilometres. Furthermore if post-emplacement serpentinization were widespread, other serpentinized units at site 334 should be coherently magnetized. Instead, individual samples have stable underlying nrms that vary in direction from sample to sample, exactly as for the unserpentinized gabbros. These units were probably magnetized before emplacement but block rotations have destroyed directional coherence of the crms or trms, except on a local scale.

Some blocks do escape rotation, as witness the site 334, unit 2 and site 395 serpentinites, but on the whole, tectonic or diapiric serpentinites emplaced at shallow crustal depths are unlikely to possess directionally coherent nrms over distances large enough to produce magnetic stripes. Serpentinites *in situ* at lower crustal depths, particularly peridotites, are a potent anomaly source, however, provided their crm was produced $\lesssim 0.5$ Ma after spreading began.

In Fig. 16, we propose a magnetic layering of the oceanic crust away from the axis that differs in a number of respects from that put forward by Kent *et al.* (1978, fig. 10). Layer 2A, with average magnetization following maghemitization of 2.5×10^{-3} emu cm^{-3} (Lowrie 1974, 1977; Harrison 1976), contributes half or less of observed anomaly amplitudes. Layer 2B (zeolite-facies and greenschist-facies doleritic sills and sheeted dykes), whose average stable magnetization is taken by Kent *et al.* to be negligible ($\approx 10^{-5}$ emu cm^{-3}) we propose as a major contributor to magnetic stripes, with a mean magnetization of 0.5×10^{-3} emu cm^{-3} and a thickness 2 or 3 times that of Layer 2A. Layer 3A (greenschist-facies and amphibolite-facies 'isotropic' gabbros) have mean magnetization of $\approx 1 \times 10^{-3}$ emu cm^{-3}, as proposed by

Kent *et al.*, but in disagreement with these authors, underlying much thicker Layer 3B (essentially unmetamorphosed cumulate gabbros) has mean magnetization of only 0.2×10^{-3} emu cm^{-3} and does not contribute appreciably to anomalies. Thus we feel Kent *et al.* have overrated Layer 3B and underrated Layer 2B as an anomaly source.

The contribution of serpentinites is more problematic. On the arbitrary assumption that a 2–3 km thick layer of the lower crust and upper mantle consists of 20 per cent by volume serpentinite with a coherent crm (i.e. crm agreeing in polarity and direction with the stable nrm of overlying Layer 2A, 2B and 3A rocks) of average intensity 5×10^{-3} emu cm^{-3}, the base of the crust and the uppermost mantle could rival shallow intrusive layers as an anomaly source. The lower boundary of this source region is determined either by the depth of the magnetite Curie point (580°C) isotherm (*cf.* Wasilewski, Thomas & Mayhew 1979) or else by the limit of serpentinization. Serpentinized cumulate gabbros (Layer 3B) and shallow diapiric serpentinites (Layers 2 and 3) are ignored. The former are magnetically weak compared to serpentinized peridotites and the latter tend to have suffered tectonic rotations and in any case comprise at most 10 per cent of the upper crust.

6 Conclusions

Our conclusions are the following.

(1) Magnetite ($T_c = 580$°C) or Ti-poor titanomagnetite ($T_c \geqslant 520$°C) is the principal magnetic mineral in oceanic intrusive rocks of all types (Layer 2B doleritic sills, Layer 3B fresh cumulate gabbros, Layer 3B serpentinized gabbros and peridotites, and Layer 4 serpentinized lherzolites). Consequently the Curie point isotherm lies at Moho depths or even deeper far from the ridge axis. Even the deep crust and upper mantle are potential contributors to oceanic magnetic anomalies.

(2) The nrm of the doleritic sills is a primary trm carried by deuterically oxidized titanomagnetite. The nrm of the fresh gabbros resides in inclusions of pure magnetite within pyroxene grains. Since the inclusions are probably a product of high-temperature deuteric alteration of pyroxene, the nrm is likely a primary trm.

(3) Maghemitization is totally absent from any of the intrusive rocks. Their magnetic signal is thus constant with time, whereas the nrm of Layer 2A pillow basalts is progressively weakened by pervasive maghemitization.

(4) Peridotites and to a lesser extent gabbros acquire an intense and directionally stable crm residing in secondary magnetite precipitated during serpentinization. Veinlets of chrome spinel within some magnetite veins may be an indication that serpentinization began at temperatures ≈ 500°C, probably in the lower crust and upper mantle.

(5) Remanence carriers, whether primary or secondary, are of single-domain or pseudo-single-domain size, judging by Q_n ratio, hysteresis properties and alternating-field behaviour, except in interior samples of the thick doleritic sill.

(6) Viscous magnetization changes during six-week storage tests in the Earth's field were minor, except in the case of interior sill samples. Long-term VRM tests remain to be carried out, however.

(7) A directionally stable component of nrm was isolated by af demagnetization in individual samples of all groups except the serpentinized lherzolites. (These latter rocks were heavily overprinted by a spurious drilling remanence.) Median destructive fields were high for the fresh gabbros (500–750 Oe) but rather low (≈ 100 Oe) for the other groups, although sufficient to ensure long-term stability of the underlying nrm.

(8) Leg 30 doleritic gabbros, Leg 37 unit 2 serpentinized cumulate peridotites and Leg 45 serpentinized lherzolites possessed well-grouped cleaned nrms, with approximately dipole

inclinations. In two cases, the nrms were reversed and could not have been acquired during the Brunhes epoch.

(9) The stable nrms of all fresh or serpentinized Leg 37 units, except unit 2, showed large between-sample dispersion. The probable cause is local block rotations during emplacement of the site 334 intrusive mélange. Serpentinization must have preceeded tectonic emplacement.

(10) Average intensities of stable nrm $\bar{J}_{nrm}$ were $\approx 0.5 \times 10^{-3}$ emu cm^{-3} for the doleritic sill (but $\gtrsim 1 \times 10^{-3}$ emu cm^{-3} for samples from the chilled margin), $\approx 0.2 \times 10^{-3}$ emu cm^{-3} for fresh cumulate gabbros, $\geqslant 0.5 \times 10^{-3}$ emu cm^{-3} for serpentinized cumulate gabbros and $\geqslant 3 \times 10^{-3}$ emu cm^{-3} for serpentinized cumulate peridotites. No estimate could be obtained for the magnetically overprinted serpentinized lherzolites, but their magnetite content (about 1 per cent by volume) is similar to that of serpentinized cumulate peridotites.

(11) These $\bar{J}_{nrm}$ values compare well with values for samples of similar lithology and metamorphic grade from ophiolite suites and seafloor dredgehauls. However the magnetic properties of Layer 2B rocks remain relatively uncertain since so few have been drilled or dredged from the seafloor and most ophiolitic equivalents have been degraded by further metamorphism during or following obduction.

(12) We propose (Fig. 16) a magnetic layering of the oceanic crust in which the significant anomaly sources are: Layer 2A (pillow-basalts), $\bar{J}_{nrm} = 2.5 \times 10^{-3}$ emu cm^{-3} following maghemitization; Layer 2B (zeolite and greenschist facies doleritic sills and sheeted dykes), $\bar{J}_{nrm} = 0.5 \times 10^{-3}$ emu cm^{-3}; Layer 3A (amphibolite facies metagabbros), $\bar{J}_{nrm} = 1 \times 10^{-3}$ cm^{-3}, and possibly a partially serpentinized peridotite layer at the base of Layer 3B and the uppermost mantle, $\bar{J}_{nrm} = 5 \times 10^{-3}$ emu cm^{-3} over an unknown volume fraction of the layer. This model differs from that of Kent *et al.* (1978) in that we include Layer 2B and a deep serpentinized region as anomaly sources but exclude most of Layer 3B (fresh cumulate gabbros).

(13) Tectonic serpentinites intruded in the middle and upper crust have probably suffered local block rotations like those inferred for our site 334 samples. If so, the resulting disruption of their nrms would render them a weak and incoherent anomaly source.

Acknowledgments

We are indebted to Cathérine Mével (Laboratoire de Pétrographie, Université de Paris VI) for petrological descriptions of our samples and many valuable discussions of the igneous and metamorphic structure of the oceanic crust. We thank also A. Perseil (Muséum National d'Histoire Naturelle, Paris) who identified the sulphides and manganese oxides and C. S. Grommé and E. A. Mankinen (U.S. Geological Survey, Menlo Park, CA) who computed the thermomagnetic curves. This work was supported by the Centre National pour l'Exploitation des Océans under grant CNEXO 77/5460. DJD was also supported by the Natural Sciences and Engineering Research Council Canada through a Travel Grant during his stay in Paris and Operating Grants during the writing-up phase in Toronto.

References

Babkine, J., Conquéré, F., Vilminot, J. C. & Phan, K. D., 1965. Les spinelles des basaltes de Monistrol d'Allier (chaîne du Devès, Haute Loire), *Bull. Soc. fr. Minér. Cristallogr.*, **88**, 447–455.

Bailey, M. E., 1975. The magnetic properties of pseudo-single-domain grains, *MSc thesis*, University of Toronto.

Banerjee, S. K., 1980. Magnetism of the oceanic crust: evidence from ophiolite complexes, *J. geophys. Res.*, **85**, 3557–3566.

Banerjee, S. K., Butler, R. F. & Stout, J. H., 1974. Magnetic properties and mineralogy of exposed oceanic crust on Macquarie Island, *J. Geophys. (Z. Geophys.)*, **40**, 537–548.

Banerjee, S. K., Levi, S. & Bogdan, D., 1977. Observations of nearly pure magnetite in the upper oceanic crust – implications for thermal regime at a spreading center (abstract), *Eos (Trans. Am. geophys. Un.)*, **58**, 379.

Beske-Diehl, S. & Banerjee, S. K., 1979. An example of magnetic properties as indicators of alteration in ancient oceanic lithosphere – the Othris ophiolite, *Earth planet. Sci. Lett.*, **44**, 451–462.

Beske-Diehl, S. & Banerjee, S. K., 1980. Metamorphism in the Troodos ophiolite: implications for marine magnetic anomalies, *Nature*, **285**, 563–564.

Bryan, W. B. & Moore, J. G., 1977. Compositional variations of young basalts in the Mid-Atlantic rift valley near lat. 36° 49′N, *Bull. geol. Soc. Am.*, **88**, 556–570.

Cann, J. R., 1968. Geological processes at mid-ocean ridge crests, *Geophys. J. R. astr. Soc.*, **15**, 331–341.

Cann, J. R., 1974. A model for oceanic crustal structure developed, *Geophys. J. R. astr. Soc.*, **39**, 169–187.

Cann, J. R., 1979. Metamorphism in the ocean crust, in *Deep Drilling Results in the Atlantic Ocean: Ocean Crust*, pp. 230–238, eds Talwani, M., Harrison, C. G. A. & Hayes, D. E., American Geophysical Union, Washington, DC.

Carmichael, C. M., 1970. The Mid-Atlantic Ridge near 45° N, VII. Magnetic properties and opaque mineralogy of dredged samples, *Can. J. Earth Sci.*, **7**, 239–256.

Caytrough, 1979. Geological and geophysical investigation of the Mid-Cayman Rise spreading center: initial results and observations, in *Deep Drilling Results in the Atlantic Ocean: Ocean Crust*, pp. 66–94, eds Talwani, M., Harrison, C. G. A. & Hayes, D. E., American Geophysical Union, Washington, DC.

Christensen, N. I. & Salisbury, M. H., 1975. Structure and constitution of the lower oceanic crust, *Rev. Geophys. Space Phys.*, **13**, 57–86.

Day, R., Fuller, M. & Schmidt, V. A., 1977. Hysteresis properties of titanomagnetites: grain-size and compositional dependence, *Phys. Earth planet. Int.*, **13**, 260–267.

Day, R. & Luyendyk, B., 1979. First paleomagnetic results from the Samail ophiolite, Oman: II. Wadi Kadir gabbro section (abstract), *Eos (Trans. Am. geophys. Un.)*, **60**, 964.

Deer, W. A., Howie, R. A. & Zussman, J., 1964. *Rock forming minerals, vol. 5 (non-silicates)*, Wiley, New York.

Dewey, J. F. & Kidd, W. S. F., 1977. Geometry of plate accretion, *Bull. geol. Soc. Am.*, **88**, 960–968.

Doell, R. R. & Cox, A., 1967. Recording magnetic balance, in *Methods in Paleomagnetism*, pp. 440–444, eds Collinson, D. W., Creer, K. M. & Runcorn, S. K., Elsevier, Amsterdam.

Dunlop, D. J., 1973. Superparamagnetic and single-domain threshold sizes in magnetite, *J. geophys. Res.*, **78**, 1780–1793.

Dunlop, D. J., 1974. Thermal enhancement of magnetic susceptibility, *J. Geophys. (Z. Geophys.)*, **40**, 439–451.

Dunlop, D. J., 1979. On the use of Zijderveld vector diagrams in multicomponent paleomagnetic studies, *Phys. Earth planet. Int.*, **20**, 12–24.

Dunlop, D. J., Hanes, J. A. & Buchan, K. L., 1973. Indices of multidomain magnetic behaviour in basic igneous rocks: alternating-field demagnetization, hysteresis and oxide petrology, *J. geophys. Res.*, **78**, 1387–1393.

Evans, M. E. & Wayman, M. L., 1970. An investigation of small magnetic particles by means of electron microscopy, *Earth planet. Sci. Lett.*, **9**, 365–370.

Flower, M. F. J., Robinson, P. T., Schmincke, H.-U. & Ohnmacht, W., 1977. Petrology and geochemistry of igneous rocks, DSDP Leg 37, in *Initial Reports of the Deep Sea Drilling Project*, **37** pp. 653–679, eds Aumento, F., Melson, W. G. *et al.*, US Government Printing Office, Washington, DC.

Fox, P. J. & Opdyke, N. D., 1973. Geology of the oceanic crust: magnetic properties of oceanic rocks, *J. geophys. Res.*, **78**, 5139–5154.

Fox, P. J., Schreiber, E. & Peterson, J. J., 1973. The geology of the oceanic crust: compressional wave velocities of oceanic rocks, *J. geophys. Res.*, **78**, 5155–5171.

Gaunt, P. J., 1960. A magnetic study of precipitation in a gold-cobalt alloy, *Phil. Mag.*, **5**, 1127–1145.

Grommé, C. S., Wright, T. L. & Peck, D. L., 1969. Magnetic properties and oxidation of iron-titanium oxide minerals in Alae and Makaopuhi lava lakes, Hawaii, *J. geophys. Res.*, **74**, 5277–5293.

Hall, J. M., 1976. Major problems regarding the magnetization of oceanic crustal layer 2, *J. geophys. Res.*, **81**, 4223–4231.

Halls, H. C., 1976. A least-squares method to find a remanence direction from converging remagnetization circles, *Geophys. J. R. astr. Soc.*, **45**, 297–304.

Harrison, C. G. A., 1976. Magnetization of the oceanic crust, *Geophys. J. R. astr. Soc.*, **47**, 257–283.

Helmstaedt, H., 1977. Postmagmatic textures and fabrics of gabbros and peridotites from DSDP site 334, in *Initial Reports of the Deep Sea Drilling Project*, **37**, pp. 757–762, eds Aumento, F., Melson, W. G. *et al.*, US Government Printing Office, Washington, DC.

Hoffman, K. A. & Day, R., 1978. Separation of multicomponent NRM: a general method, *Earth planet. Sci. Lett.*, **40**, 433–438.

Irving, E., Robertson, W. A. & Aumento, F., 1970. The Mid-Atlantic Ridge near 45° N, VI. Remanent intensity, susceptibility and iron content of dredged samples, *Can. J. Earth Sci.*, **7**, 226–238.

Johnson, H. P. & Atwater, T., 1977. Magnetic study of basalts from the Mid-Atlantic Ridge, lat. 37°N, *Bull. geol. Soc. Am.*, **88**, 637–647.

Johnson, H. P., Lowrie, W. & Kent, D. V., 1975. Stability of anhysteretic remanent magnetization in fine and coarse magnetite and maghemite particles, *Geophys. J. R. astr. Soc.*, **41**, 1–10.

Kent, D. V., Honnorez, B. M., Opdyke, N. D. & Fox, P. J., 1978. Magnetic properties of dredged oceanic gabbros and the source of marine magnetic anomalies, *Geophys. J. R. astr. Soc.*, **55**, 513–537.

Larson, E. E., Ozima, M., Ozima, M., Nagata, T. & Strangway, D. W., 1969. Stability of remanent magnetization of igneous rocks, *Geophys. J. R. astr. Soc.*, **17**, 263–292.

Levi, S. & Banerjee, S. K., 1977. The effects of alteration on the natural remanent magnetization of three ophiolite complexes: possible implications for the oceanic crust, *J. Geomagn. Geoelect.*, **29**, 421–439.

Levi, S., Banerjee, S. K., Beske-Diehl, S. & Moskovitz, B., 1978. Limitations of ophiolite complexes as models for the magnetic layer of the oceanic lithosphere, *Geophys. Res. Lett.*, **5**, 473–476.

Lienert, B. R. & Wasilewski, P. J., 1979. A magnetic study of the serpentinization process, *Earth planet. Sci. Lett.*, **43**, 406–416.

Lister, C. R. B., 1972. On the thermal balance of a mid-oceanic ridge, *Geophys. J. R. astr. Soc.*, **26**, 515–535.

Lowrie, W., 1974. Oceanic basalt magnetic properties and the Vine and Matthews hypothesis, *J. Geophys. (Z. Geophys.)*, **40**, 513–536.

Lowrie, W., 1977. Intensity and direction of magnetization in oceanic basalts, *J. geol. Soc. London*, **133**, 61–82.

Lowrie, W. & Fuller, M., 1971. On the alternating field demagnetization characteristics of multidomain thermoremanent magnetization in magnetite, *J. geophys. Res.*, **76**, 6339–6349.

Lowrie, W. & Kent, D. V., 1978. Characteristics of VRM in oceanic basalts, *J. Geophys. (Z. Geophys)*, **44**, 297–315.

MacLean, W. H., 1977. Sulphides in the core from Leg 37 drill holes, in *Initial Reports of the Deep Sea Drilling Project*, **37**, pp. 875–881, eds Aumento, F., Melson, W. G. *et al.*, US Government Printing Office, Washington, DC.

Park, J. K. & Irving, E., 1970. The Mid-Atlantic Ridge near 45° N, XII. Coercivity, secondary magnetization, polarity, and thermal stability of dredge samples, *Can. J. Earth Sci.*, **7**, 1499–1538.

Parry, L. G., 1965. Magnetic properties of dispersed magnetite powders, *Phil. Mag.*, **11**, 302–312.

Peterson, J. J., Fox, P. J. & Schreiber, E., 1974. Newfoundland ophiolites and the geology of the oceanic layer, *Nature*, **247**, 194–196.

Prévot, M., 1981. Some aspects of magnetic viscosity in subaerial and submarine volcanic rocks, *Geophys. J. R. astr. Soc.*, **66**, 169–192.

Prévot, M. & Grommé, C. S., 1975. Intensity of magnetization of subaerial and submarine basalts and its possible change with time, *Geophys. J. R. astr. Soc.*, **40**, 207–224.

Prévot, M., Lecaille, A. & Hekinian, R., 1979. Magnetism of the Mid-Atlantic Ridge crest near 37° N from FAMOUS and DSDP results: a review, in *Deep Drilling Results in the Atlantic Ocean: Ocean Crust*, pp. 210–229, eds Talwani, M., Harrison, C. G. A. & Hayes, D. E., American Geophysical Union, Washington, DC.

Prévot, M., Lecaille, A. & Mankinen, E. A., 1981. Magnetic effects of maghemitization of oceanic crust, *J. geophys. Res.*, **86**, 4009–4020.

Rahman, A. A., Duncan, A. D. & Parry, L. G., 1973. Magnetization of multidomain magnetite particles, *Riv. Ital. Geofis.*, **22**, 259–266.

Saad, A. H., 1969. Magnetic properties of ultramafic rocks from Red Mountain, California, *Geophys.*, **34**, 974–987.

Schwarz, E. J., 1973. Magnetic characteristics of massive sulphide ore bodies near Sudbury, Canada, *Can. J. Earth Sci.*, **10**, 1735–1743.

Stacey, F. D., 1967. The Koenigsberger ratio and the nature of thermoremanence in igneous rocks, *Earth planet. Sci. Lett.*, **2**, 67–68.

Stern, C., deWit, M. J. & Lawrence, J. R., 1976. Igneous and metamorphic processes associated with the formation of Chilean ophiolites and their implication for ocean floor metamorphism, seismic layering, and magnetism, *J. geophys. Res.*, **81**, 4370–4380.

Stoeser, D. B., 1975. Igneous rocks from Leg 30 of the Deep Sea Drilling Project, in *Initial Report of the Deep Sea Drilling Project*, **30**, pp. 401–414, eds Andrews, J. E., Packham, G. & Herring, J., US Government Printing Office, Washington, DC.

Talwani, M., Windisch, C. C. & Langseth, M. G., 1971. Reykjanes ridge crest: a detailed geophysical study, *J. geophys. Res.*, **76**, 473–517.

Thellier, E., 1967. A big sample spinner magnetometer, in *Methods in Paleomagnetism*, pp. 149–154, eds Collinson, D. W., Creer, K. M. & Runcorn, S. K., Elsevier, Amsterdam.

Vine, F. J. & Moores, E. M., 1972. Model for the gross structure, petrology, and magnetic properties of oceanic crust, *Mem. geol. Soc. Am.*, **132**, 195–205.

Vine, F. J. & Wilson, J. T., 1965. Magnetic anomalies over a young ocean ridge off Vancouver Island, *Science*, **150**, 485–489.

Wasilewski, P. J., Thomas, H. H. & Mayhew, M. A., 1979. The Moho as a magnetic boundary, *Geophys. Res. Lett.*, **6**, 541–544.

Wohlfarth, E. P., 1958. Relations between different modes of acquisition of the remanent magnetization of ferromagnetic particles, *J. appl. Phys.*, **29**, 595–596.

Zijderveld, J. D. A., 1967. A.C. demagnetization of rocks: analysis of results, in *Methods in Paleomagnetism*, pp. 254–286, eds Collinson, D. W., Creer, K. M. & Runcorn, S. K., Elsevier, Amsterdam.

Zijderveld, J. D. A., 1975. Paleomagnetism of the Esterel rocks, *PhD thesis*, State University of Utrecht.